STATISTICAL CORRELATION AS A TOOL IN PROPAGATION STUDIES

by

Robert L. Lyall, Jr.

Thesis submitted to the Faculty of the

Virginia Polytechnic Institute and State University

in partial fulfillment of the requirements for the degree of

MASTER OF SCIENCE

in

Electrical Engineering

APPROVED:

C. W. Bostian, Chairman

I. M. Besieris

E. A. Manus

T. Pratt

May, 1982

Blacksburg, Virginia

ACKNOWLEDGEMENTS

I would like to express my deep appreciation to the people who made this thesis possible. Special thanks go to my committee chairman, Dr. C. W. Bostian, whose guidance and assistance was a great asset. I would also like to thank my other committee members, Dr. I. M. Besieris, Dr. E. A. Manus, and Dr. T. Pratt, whose comments and suggestions were very helpful.

I would like to express my appreciation to Dr. K. Hinklemann, whose assistance in the area of statistics was beneficial. Thanks also go to Cynthia R. Will, whose expertise and patience in typing this work are greatly appreciated.

Finally, I wish to express my sincere love and appreciation to my wife Cathy, and my parents, whose love and encouragement were invaluable.

TABLE OF CONTENTS

Page

LIST OF FIGURES

Page

Chapter I

USING STATISTICAL CORRELATION IN RADAR MEASUREMENTS

1.1 INTRODUCTION

The growing use of satellites in communications systems has brought about the need for more operating space in the frequency spectrum. This need can be met by expansion into the frequencies above 10 GHz. However, as operating frequencies increase above 10 GHz, the effects of hydrometeors such as rain and ice become severe.

Radar can be used to provide more information about hydrometeors existing in the propagation path. Single polarized radar has been used to detect the presence of ice in the propagation path [1][2][3] and also to predict attenuation along the propagation path. [4] Dual polarized radar has been used as a tool in the study of millimeter wave propagation [5][6][7] and also to predict slant path attenuation. [8] [9] The usefulness of radar in propagation research has been proven.

This thesis is an extension of previous work in which radar backscatter was statistically correlated with received satellite signals to provide evidence of ice in the propagation path. [3] In the work reported here, variables diffe-

rent than those used in the previous work are correlated and different results are obtained.

Background material on depolarization and radar meteorology is presented in the Appendix.

1.2 DISCUSSION OF PREVIOUS WORK

The only previous work in the area of statistically correlating radar backscatter quantities with satellite signal quantities was performed by P. F. Shutie, J. E. Allnutt and E. G. Mackenzie and published in 1977. [3] In that paper, analysis of an event which occured on 5 May 1976 and lasted approximately 2 hours was reported. The authors used the ATS-6 satellite downlink (both co- and cross-polarized signals were recorded) and a colocated fixed-path radar operating at 9.45 GHz. The elevation angle was 22.4 degrees and the downlink frequency was 30 GHz. The propagation path was sampled out to 22.5 km in .5 km sections. One complete radar scan took 12.5s and data was stored on magnetic tape along with satellite signal xpd values. The radar data and satellite signal data were analyzed statistically at a later date.

Before the correlation analysis was performed, the radar data were range corrected. Range correcting takes the $\frac{1}{r^2}$ factor in the reflected power into account. Radar range

gates are "weighted" according to their range. Thus, the significance of backscattered power from the gates can be compared more easily. The satellite signal data were used to compute the xpd, defined as the ratio of the wanted co-polarized signal to the unwanted cross-polarized signal. The range-corrected backscatter was averaged over one kilometer intervals and variations in radar backscatter were correlated with xpd fluctuations. No reason was given for correlating variations in the signals, as opposed to absolute signal levels. One explanation might be that the radar used in the experiment was not calibrated. However, a calibration is not required for correlating absolute quantities. The correlation analysis was performed for successive 160 second intervals; then an average correlation coefficient was computed for each range gate. The averaging process was not given in the publication. The analysis of only one event was published.

Successful results were obtained using the correlation analysis previously described. For the event analyzed in the publication, ice was determined to be the cause of the depolarization. Shutie, Allnutt, and Mackenzie's paper was very influential at the time of publication. It played an important part in establishing that anomalous depolarization, as it was called then, was in fact due to ice. But

since then, no further work in the area of applying statistical correlation techniques to propagation studies has been reported. This thesis continues where they stopped and examines statistical correlation as a tool in radar studies of propagation.

1.3 SUMMARY OF THE CORRELATION ANALYSIS PRESENTED IN THIS THESIS

The correlation technique presented in this thesis is an extension of the work discussed in Section 1.2. The correlation analysis reported by Shutie et al. was performed specifically to produce evidence supporting ice depolarization. This thesis goes further and uses correlation analysis as a technique for determining the type of propagation event being analyzed. Basically, correlation identifies the radar range gates in which backscatter has the same time dependence as the satellite signal quantities.

The VPI&SU 11.6 GHz SIRIO receiving system [10] is the source for the satellite signals analyzed in this thesis. The source of radar signals is a colocated S band radar operating at 2.8 Ghz (λ = 10.714 cm). The elevation angle is 11.08 degrees. Both satellite data and radar data are recorded on a computer disk and analyzed at a later date. The recorded satellite signal data which are indirectly used in

the correlation analysis are the co- and cross-polarized signal levels in dBm, called "co and cross" here. These are measured at the 1.05 GHz i.f. section of the SIRIO receiver. The recorded radar data are signals from each of the 128 range gates (1 gate = 0.5 km). The satellite signal quantities used in the analysis are the co signal attenuation and the polarization isolation. The attenuation is given by

$$\text{Attenuation} = C_1 - \text{CO} \tag{1.1}$$

where C_1 is the clear weather value of the CO signal. Isolation is given as

$$\text{Isolation} = \text{CO} - \text{CROSS} + C_2 \tag{1.2}$$

where C_2 is the channel gain difference in the system. Each satellite signal (co or cross) is recorded when either changes by 0.7 dB. Each signal from 128 radar range gates is recorded for a change of 4 counts up to gate 20 and a change of 1 count past gate 20. These correspond to approximately 1 dBZ and .25 dBZ respectively, where dBZ is the radar reflectivity factor Z (mm^6/m^3) expressed in decibels. This dB form of Z is referred to Z = 1 mm^6/m^3, i.e. 0 dBZ =

1 mm^6/m^3. Z is given by

$$Z = \frac{1}{C} \frac{r^2}{|K|^2} \overline{P}_r \quad , \tag{1.3}$$

where $\overline{P}_r$ is the received power, $|K|^2$ is a form of the complex index of refraction of the target, r is the distance to the target and C is a constant associated with the radar system. These recorded data are later processed and a record which includes the satellite signals and the radar signals is updated for each time a data point was recorded.

The correlation analysis presented in this thesis is significantly different from that discussed in Section 1.2. Both attenuation and isolation (xpd) in dB are correlated with radar backscatter in dBZ. Another important difference is that absolute signal values (as opposed to changes in signal values) are correlated. Also, no averaging was performed on the correlation coefficients. The Pearson product-moment correlation coefficient is computed for each radar range gate. For each correlation coefficient, a significance probability is also computed. This is the probability that the coefficient occurred because of a chance fluctuation in the data; it is an indication of the statistical significance of the coefficient. The significance probabilities for the earlier work were not published.

The patterns produced by plotting the attenuation and isolation coefficients versus range gate number have different characteristics for different types of propagation events. The three event types are ice-induced depolarization, rain-induced attenuation/depolarization and rain attenuation (no depolarization fluctuation); each have expected correlation coefficient patterns. Correlation patterns computed from actual data agree well with expected patterns.

Chapter II

THE PEARSON PRODUCT-MOMENT CORRELATION COEFFICIENT

2.1 INTRODUCTION

The meaning of the term correlation varies with the intended use. In signal analysis, correlation may be defined as a determination of the mutual characteristics that are contained in two or more signals. Some of the various measures of correlation are correlation coefficients, correlation efficiency, correlation time, correlation bandwidth and correlation functions. [11]

The correlation analysis done in this thesis on radar backscatter and received satellite signals produces a normalized Pearson product-moment correlation coefficient. [12] Normalization takes the amplitude characteristic out of the signals being compared and is done because the two signals being correlated may have the same form but greatly different amplitudes; it makes the correlation more sensitive to the mutual characteristics of the signals. The computer program used to calculate the Pearson correlation coefficient is included in a statistics software package called SAS. [12] This package exists in the VPI&SU computing system.

2.2 VALIDITY OF THE CORRELATION COEFFICIENT: SAMPLE SIZE

The correlation work done in this thesis relates the instantaneous radar backscatter from each radar range gate (in dBZ) with the instantaneous attenuation and polarization isolation in dB measured on the SIRIO downlink. The correlation coefficient is computed with sampled values of data; the sample size required depends on the reliability desired in the correlation coefficient. We may determine the sample size by treating the satellite signals and radar backscatter as random variables and deriving the concept of the correlation coefficient being used. A discussion of this process follows. It does not give detailed theory with proofs; these are available in a standard text. [13]

A random variable is a rule that assigns a real number to each of the possible outcomes of an experiment. Let the outcomes of an experiment be denoted by the variable λ_i. These are not necessarily numbers. $X(\lambda_i)$ is a rule that assigns a real number to the outcome λ_i. $X(\lambda_i)$ is a random variable. It may be continuous or discrete.

A cumulative distribution function relates the outcome probabilities of a random variable to the random variable. The cumulative distribution function for the random variable

$X(\lambda)$ is defined as

$$F_X(x) \equiv P\ X(\lambda) \leq x\} \tag{2.1}$$

where $-\infty < x < \infty$. For a given x, $F_X(x)$ is the probability of the event $\{X(\lambda) \leq x\}$ consisting of all outcomes such that $X(\lambda) \leq x$. For the discrete random variable case, the cumulative distribution function is given as

$$F_X(x) = \sum_i P_i\ U(x - x_i) \tag{2.2}$$

where U is the unit step function and $P_i = P\{X \leq x_i\}$. The derivative of the cumulative distribution function is the probability density function of the random variable $X(\lambda)$ and is denoted by

$$p_X(x) = \frac{d}{dx}\left(F_X(x)\right) \tag{2.3}$$

The probability density function is easily extended to the discrete case. From (2) and (3),

$$p_X(x) = \frac{d}{dx}\left[\sum_i P_i\ U(x - x_i)\right] \tag{2.4}$$

$$p_X(x) = \sum_i P_i \frac{d}{dx}\ U(x - x_i) \tag{2.5}$$

$$p_X(x) = \sum_i P_i \, \delta(x - x_i) \tag{2.6}$$

where δ is the delta (or impulse) function. The area under the curve of the probability density function is the probability of occurrence of an outcome within a certain range.

Statistical averaging can be used to compute the mean value m (also called the first moment M or the expected value $E\{X\}$) of the random variable X. For the cases of a continuous random variable, integration over the entire range of $X(\lambda)$ gives

$$M_X = \int_{-\infty}^{\infty} x \, p(x) \, dx \tag{2.7}$$

For the discrete case,

$$M_X = \int_{-\infty}^{\infty} x \sum_{i=1}^{N} P_i \, \delta(x - x_i) \, dx \tag{2.8}$$

For equally probable events, $P_i = \frac{1}{N}$

$$M_X = \frac{1}{N} \int_{-\infty}^{\infty} x \sum_{i=1}^{N} \delta(x - x_i) \, dx \tag{2.9}$$

$$M_X = \frac{1}{N} \sum_{i=1}^{N} \int_{-\infty}^{\infty} x\, \delta(x - x_i)\, dx \tag{2.10}$$

$$M_X = \frac{1}{N} \sum_{i=1}^{N} x_i \tag{2.11}$$

This is the statistical average for N observations of the random variable $X(\lambda)$ with equal probability of occurence. It is also the arithmetic average.

The expected value of $X^2(\lambda)$ ($E\{X^2\}$), also known as the second moment, is given as

$$E\{X^2\} = \int_{-\infty}^{\infty} x^2\, p(x)\, dx \tag{2.12}$$

The variance of the random variable $X(\lambda)$ is found by subtracting the first moment m_x from X before computing the second moment. The variance is denoted by σ_x^2.

$$\sigma_X^2 = E\{(X - m_X)^2\} = \int_{-\infty}^{\infty} (x - m_X)^2\, p(x)\, dx \tag{2.13}$$

For the discrete case

$$E\{X^2\} = \int_{-\infty}^{\infty} x^2 \sum_{i=1}^{N} P_i\, \delta(x - x_i)\, dx \tag{2.14}$$

From (2.14), the variance for the discrete case is

$$\sigma_X^2 = \int_{-\infty}^{\infty} (x - m_X)^2 \sum_{i=1}^{N} P_i \, \delta(x - x_i) \, dx \tag{2.15}$$

$$\sigma_X^2 = \sum_{i=1}^{N} (x - m_X)^2 \, P_i \tag{2.16}$$

For the equal probability case, $P_i = \frac{1}{N}$ and

$$\sigma_X^2 = \frac{1}{N} \sum_{i=1}^{N} (x_i - m_X)^2 \tag{2.17}$$

So far, only a one-dimensional random variable has been discussed. The quantities previously discussed can be extended to include two-dimensional random variables. For example, if $X(\lambda)$ and $Y(\lambda)$ are random variables, the covariance C is defined as

$$C \equiv E\{(X - m_X)(Y - m_Y)\} \tag{2.18}$$

This is similar to the variance σ_X^2 in the one dimensional case.

$$E\{(X - m_X)(Y - m_Y) = \int_{-\infty}^{\infty}\int_{-\infty}^{\infty} (x - m_X)(y - m_Y) p_{xy}(x, y) \, dx \, dy \tag{2.19}$$

where $p_{XY}(x, y)$ is given as

$$p_{XY}(x, y) = p_X(x)\, p(y|x) = p_Y(y)p(x|y) \tag{2.20}$$

The expressions $p(y|x)$ and $p(x|y)$ are the conditional density functions. The expression $p_{XY}(x, y)$ is the joint probability density function and is defined as

$$p_{XY}(x, y) = \frac{d}{dx\, dy} F_{XY}(x, y) \tag{2.21}$$

where $F_{XY}(x, y)$, the joint cumulative probability distribution function, is given as

$$F_{XY}(x, y) = P\{X \leq x, Y \leq y\} \tag{2.22}$$

For the discrete case, the covariance is given as

$$C = \frac{1}{N} \sum_{i=1}^{N} (x_i - m_X)(y_i - m_Y) \tag{2.23}$$

All of the preceding discussion of random variables leads to the definition of the correlation coefficient ρ.

The correlation coefficient is a normalized covariance given by

$$\rho = \frac{C}{\sigma_X\, \sigma_Y} \tag{2.24}$$

The correlation coefficient ρ is a measure of how dependent the variables x and y are on each other. If the two random variables are completely dependent (perfectly linear), then the coefficient equals either +1.0 or -1.0. If the two random variables are uncorrelated, then $\rho = 0$. The limits of ρ are

$$-1 \leq \rho \leq 1 \tag{2.25}$$

Two random variables can be statistically dependent and still have a correlation coefficient of zero. But if two random variables are statistically independent of each other, then the covariance is zero and the random variables are said to be uncorrelated.

The discrete form used to compute ρ is given below. [14]

$$\rho = \frac{\sum_{i=1}^{N} (x_i - m_X)(y_i - m_Y)}{\left[\sum_{i=1}^{N} (x_i - m_X)\,(y_i - m_Y)^2\right]^{1/2}} \tag{2.26}$$

This form of the correlation coefficient can be obtained using any type of distribution. [15] For a population of data, the true value of the coefficient ρ is specified as ρ_o. For a sample of data (i.e. a subset) from this population, an estimate value of ρ is specified as r.

For comparison and computational reasons, the variable r will be transformed into another variable w.

$$w = \frac{1}{2} \ln \left[\frac{1 + r}{1 - r} \right] \tag{2.27}$$

As previously stated, the received satellite signals and radar backscatter are treated as random variables. Because the estimate correlation coefficient is computed using these random variables, it too is a random variable. The variable w has an approximately normal distribution with mean value and variance σ_w^2 given by

$$\mu_w = \frac{1}{2} \ln \left[\frac{1 + P_o}{1 - P_o} \right] \tag{2.28}$$

ρ_o is the correlation coefficent of the entire population.

$$\sigma_w^2 = \frac{1}{N - 3} \tag{2.29}$$

N is the size of the sample. [16]

The major advantage of this transformation is the interpretation of w can be made in terms of a normal distribution curve, regardless of the sample size used. Values of w in random samples are distributed almost normally, so the interpretation of σ_w is more meaningful. [15]

The parameter r is a random variable, so w is also a random variable. As previously stated, w has an approximately normal distribution.

At this point, the standardized variable Z will be introduced.

$$Z = \frac{w - \mu_w}{\sigma_w} \tag{2.30}$$

Z is used to obtain a more convenient form of the normal distribution. The value of Z that corresponds to a probability of

$$P(Z) = 1 - \alpha \tag{2.31}$$

is Z_α.

$$P(Z_\alpha) = \int_{-\infty}^{Z_\alpha} p(Z)\, dZ = P_{ROB}[Z \leq Z\ ] = 1 - \alpha \tag{2.32}$$

$$1 - P(Z_\alpha) = \int_{Z_\alpha}^{\infty} p(Z)\, dZ = P_{ROB}[Z > Z_\alpha] = \alpha \tag{2.33}$$

where $p(Z) = (\sqrt{2\pi})^{-1}\ e^{-Z^2/2}$ is the standardized density function.

The parameter r is an estimate of ρ, the correlation coefficient. This estimate is computed from a sample size

of N data pairs. This sample size is less than the population size. The actual value of ρ is ρ_o. This is the correlation coefficient for the population. It is very likely that ρ_o will not equal r.

The variables ρ, r and ρ_o will be transformed to the standardized variable Z. The variable ρ is transformed to Z, r to Z_r and ρ_o to Z_o. This will be done using the transformation from one variable to w then w to Z as previously discussed. If it is hypothesized that Z equals Z_o, how much of a difference between Z_o and Z_r should be accepted before the hypothesis of $Z = Z_o$ be rejected? This can be answered using the sampling distribution of the estimate Z_r. The probability of a specific difference between Z_r and Z_o, based on the sampling distribution, must be considered. If the probability of a difference is large, the difference would not be significant and therefore the hypothesis that $Z = Z_o$ would be accepted. By similar reasoning, if the probablity of a difference is small, the difference would be significant and the hypothesis that $Z = Z_o$ would be rejected.

Suppose the estimate Z_r has a probability density function $p(Z_r)$ as shown in Fig. 2-1. If $Z = Z_r$, then $p(Z_r)$ has

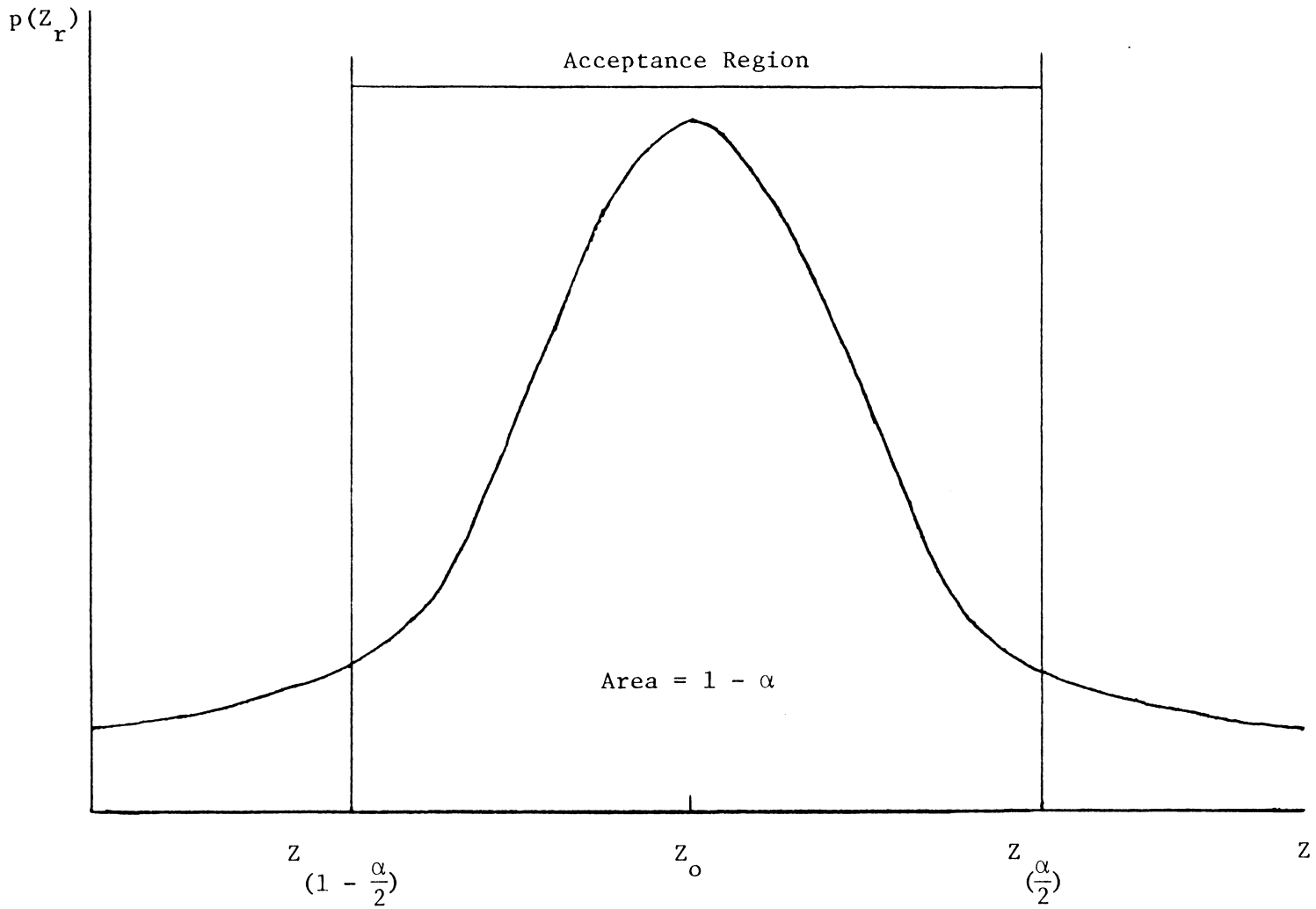

Figure 2-1. Probability density function for Z_r.

an average value of Z_o.

$$\text{PROB}[Z_r \leq Z_{1-\frac{\alpha}{2}}] = \int_{-\infty}^{Z_{1-\frac{\alpha}{2}}} p(Z_r)\, dZ_r = \frac{\alpha}{2} \tag{2.34}$$

where $\alpha/2$ is the area under the curve from $Z_{1-\frac{\alpha}{2}}$ to $-\infty$. This is the probability the Z_r will fall below the $Z_{\frac{\alpha}{2}}$ level. Similarly,

$$\text{PROB}[Z_r > Z_{\frac{\alpha}{2}}] = \int_{Z_{\frac{\alpha}{2}}}^{\infty} p(Z_r)\, dZ_r = \frac{\alpha}{2} \tag{2.35}$$

where, again, $\alpha/2$ is the area under the curve from $Z_{\frac{\alpha}{2}}$ to ∞. This is the probability that Z_r will be above the $Z_{\frac{\alpha}{2}}$ level. The total probability that Z_r will be outside the range $Z_{1-\frac{\alpha}{2}}$ to $Z_{\frac{\alpha}{2}}$ is $\alpha/2 + \alpha/2 = \alpha$.

Suppose that α is so small that Z_r being outside the range, $Z_{1-\frac{\alpha}{2}}$ to $Z_{\frac{\alpha}{2}}$ is very unlikely. If Z_r did fall outside this range, then there would be good reason to question the hypothesis that $Z = Z_o$. (Such a value of Z_r would be unlikely if the hypothesis were accepted.) If Z_r did not fall in the range $Z_{1-\frac{\alpha}{2}}$ to $Z_{\frac{\alpha}{2}}$, , there is no good reason to question the hypothesis $Z = Z_o$ and it would be accepted.

Two possible errors can occur when making hypothesis tests: (1) the hypothesis can be rejected when it is actually true and (2) the hypothesis can be accepted when it is

actually false. Error (1) would occur if the hypothesis that $Z = Z_o$ was true and Z_r fell in the rejection region. The probability of this happening is α, i.e. α is the probability of error (1) occuring.

The probability of error (2) occuring is also important. Suppose $Z = Z_o + d$ or $Z = Z_o - d$ where d is a specified deviation of Z from the hypothesized value Z_o. If $Z = Z_o \pm d$ and it is hypothesized $Z = Z_o$, then the probability of Z_r being in the acceptance region between $Z_{1-\frac{\alpha}{2}}$ and $Z_{\frac{\alpha}{2}}$ is β. So, the probability of error (2) is β. This is the probability of detecting a difference $\pm d$ from the hypothesized value Z_o.

For a specific sample size N, the probability of error (1) can be reduced by reducing the level of α. But, this in turn increases the probability of error (2), β. The only way to reduce both α and β is to increase the sample size N used to make the estimate Z_r. [16]

The sample size N can be computed using the sampling distribution of Z. Let

$$w_o = \frac{1}{2} \ln \left[\frac{1 + P_o}{1 - P_o} \right] \tag{2.36}$$

and

$$w = \frac{1}{2} \ln \left[\frac{1 + r}{1 - r} \right] \tag{2.37}$$

$$d = w_o - w \tag{2.38}$$

Now, the standardized variable Z discussed previously will be used. Z has the form

$$Z = \frac{X - \mu_x}{\sigma_x} \quad , \tag{2.39}$$

where X is the variable being transformed, μ_x is the mean of the variable and σ_x is the standard deviation.

This can be applied to the variables w_{LO} and w_{HI} which are the transformed r values corresponding to $Z_{1-\alpha}$ and Z_α respectively.

$$Z_{1-\alpha} = \frac{w_{LO} - \mu_w}{\sigma_w} = - Z_\alpha \tag{2.40}$$

$$Z_\alpha = \frac{w_{HI} - \mu_w}{\sigma_w} \tag{2.41}$$

From these,

$$w_{LO} = (- Z_\alpha) \sigma_w + \mu_w \tag{2.42}$$

$$w_{HI} = (Z_\alpha)\ \sigma_w + \mu_w \tag{2.43}$$

Also,

$$w_{LO} = Z_\beta\ \sigma_w + \mu_w - d \tag{2.44}$$

$$w_{HI} = Z_\beta\ \sigma_w + \mu_w + d \tag{2.45}$$

Equating the two w_{LO} equations,

$$- Z_\alpha\ \sigma_w + \mu_w = Z_\beta\ \sigma_w + \mu_w - d \tag{2.46}$$

$$Z_\beta\ \sigma_w + Z_\alpha\ \sigma_w = d \tag{2.47}$$

$$(Z_\beta + Z_\alpha)\ \sigma_w = d \tag{2.48}$$

$$\frac{Z_\beta + Z_\alpha}{w_o - w} = \frac{1}{\sigma_w} \tag{2.49}$$

$$\frac{Z_\beta + Z_\alpha}{w_o - w} \tag{2.50}$$

$$N = 3 + \left[\frac{Z_\beta + Z_\alpha}{w_o - w}\right] \tag{2.51}$$

This is the minimum number of data pairs needed in a sample taken from the entire population. The probability of occurence of error (1) and error (2) decreases as N increases.

The number of data pairs needed in a sample depends on the confidence desired in the correlation coefficient computed from the sample. N could be computed by first choosing the probabilities α for error (1) and β for error (2). Once these are chosen, they are transformed to the standardized variable Z using a table of normal distributions. Next, the correlation coefficient ρ_o for the entire population is computed and transformed to w_o. Now, the remaining variable in the equation for computing N is , the estimate of the correlation coefficient. A maximum value of r could be transformed to w and the minimum number of data pairs needed could be computed. This r is less than the actual correlation coefficient ρ_o of the population. As previously stated, N can be increased in order to reduce the probability of occurence of the two errors.

The correlation coefficient computed from N data pairs can be checked for significance. If it is hypothesized that the true correlation coefficient is zero, r values differing from zero in the samples are obtained. An estimate of the

standard deviation σ_r of the set of r values is given as

$$\sigma_r = \frac{1}{\sqrt{N - 1}} \tag{2.52}$$

where N is the number of data pairs in the sample. To be sure that r is a significant estimate and not a coefficient that may have arisen by chance, r should be at least three times greater than σ_r. [15]

2.3 VALIDITY OF THE CORRELATION COEFFICIENT IN TERMS OF THE SIGNIFICANCE PROBABILITY

A more meaningful and more accurate check for the significance of a correlation coefficient can be made using the t test. Once the correlation coefficient is computed, it should be checked for statistical significance, i.e. the possibility that it arose from chance fluctuations in the data. The t test is performed by hypothesizing the actual correlation coefficient ρ_o is zero. This hypothesis implies the estimate r is caused by chance fluctuation in the data. If $\rho_o = 0$, then the sampling distribution of r is normal, provided N is not too small. The hypothesis $\rho_o = 0$ is checked using the t test, which also has a normal distribution. r is transformed to t using

$$t = \frac{r\sqrt{N - 2}}{\sqrt{1 - r^2}} \tag{2.53}$$

When the hypothesis $\rho_o = 0$ is true, t is distributed in accordance with tabulated values of t with degrees of freedom df equal to N-2. The t test proceeds as follows.

The estimate r is computed and transformed to t. Let this value be t_r. Tables of significant t values (t_s), their associated probability γ and the degree of freedom (df) are used to check the statistical significance of t . The df value, N-2, is known. The value of γ is the probability of $t_r \geq t_s$. For a given df, each t_s has an associated γ. If $\rho_o = 0$, the distribution of t is symmetric and the probability of $t_r \leq -t_s$ is γ. So the prob $[t_r \leq -t_s]$ or prob $[t_r \geq t_s]$ is $\gamma + \gamma = 2\gamma$. If $\rho_o = 0$ then prob $[t_r \geq t_s] = \gamma$. If γ is small and $t_r \geq t_s$ then the hypothesis $\rho_o = 0$ must be rejected and r is significant with significance probabiity 2γ. This is the probability of the estimate r being due to chance fluctuation in the data. [17] This significance probability is computed in the SAS procedure CORR, which is used to compute the Pearson product moment correlations. [12] The significance probabilities computed in the SAS procedure are more accurate than those obtained from a table. An example will clarify the process described above.

For N= 32, the degree of freedom, df, is 32 - 2 = 30. Suppose r = 0.85. The value of t_r is

$$t_r = \frac{0.85\sqrt{32 - 2}}{\sqrt{1 - (0.85)^2}} = 8.84$$

Next, the table of t values is used to get t_s. For df = 30, t_s = 2.75 is the largest value of t_s avaiable from the chart. The probability of $t \geq 2.75$ or $t \leq -2.75$ is 2(0.005) = 0.01. 8.84 is greater than 2.75, so the hypothesis that = 0 is rejected and the estimate r is significant.

2.4 CHOICE OF THE METHOD FOR DETERMINING SIGNIFICANCE

Two possible methods for determining the significance of the correlation coefficient have been discussed. Both methods could be used. However, for simplicity, only one will be used in the correlation analysis.

The first method discussed produces the number of observations required to provide a given degree of accuracy. This was a function of the probability of each error type (1 and 2) occuring and the desired difference in the actual correlation coefficient (computed from the total population) and the correlation coefficient being computed. The second method produced the probability of the computed correlation coefficient occuring from chance fluctuation in the data. This was done using the t test and was included in the SAS program package.

The first method is more difficult to apply; it requires the computation of the actual correlation coefficient (for the total population). Also, the other inputs mentioned

above must be provided. The second method requires no other inputs from the user; it is computed with the correlation coefficient. No minimum or maximum sample size is required to use the second method, so any sample size can be used. If the significance probabilities are too high for a given sample size, the sample size can be increased possibly to decrease the significance probabilities. Because of its ease of application, the second method will be used.

Chapter III

EXPECTED CORRELATION PATTERNS

3.1 INTRODUCTION

The work of this thesis involves correlating linear functions of the satellite signals with the radar backscatter in dBZ. The value of the Pearson product-moment correlation coefficient is an indication of how dependent the variables are on each other. In the correlation calculation, satellite signal attenuation in dB and satellite signal isolation in dB are correlated with the backscatter in dBZ from each radar range gate, where each gate is 500 m in length. Thus, each gate has two correlation coefficients associated with it, one for attenuation and the other for isolation. There are 128 radar range gates, so it is possible to have 128 pairs of correlation coefficients. However, the limitations of the radar system restrict the number of gates that produce valid coefficients in the correlation calculations. Ground clutter contaminates the data in approximately the first 20 gates, making the validity of the correlation coefficients of these gates questionable. The amount of precipitation in these gates makes a difference in the amount of contamination. For example, a heavy rain rate would over-

ride any contamination from ground clutter, where as a light rain may not. The sensitivity of the radar causes problems in the outer gates. The noise floor increases with an r^2 dependence, causing return from the outer gates to fluctuate; signals above the noise floor are recorded while signals below the noise floor are not. In some cases, this noise problem impairs the ability to locate ice along the path.

3.2 CHOICE OF VARIABLES TO CORRELATE

As stated above, the satellite signal attenuation and isolation are used to calculate the coefficients. The co-polar and cross-polar signal values could have been used instead and the same information obtained. For example, during an ice-crystal depolarization event, the attenuation stays almost constant while the isolation fluctuates due to depolarization. The attenuation is the co-polar signal added to a constant (clear weather co-polar signal level), so it gives the same information as the co-polar signal. The isolation changes are then due to changes in the cross-polar signal, thus the isolation gives the same information as the cross-polar signal. The patterns of the correlation coefficient calculated using co-polar and cross-polar signal are different from those calculated using attenuation and isola-

tion; however, they give the same information. Attenuation and isolation are quantities usually presented. For this reason, the isolation and attenuation will be used in the correlation coefficient calculations.

3.3 PROPAGATION EVENT CLASSIFICATION

There are three types of propagation events expected. Two are associated with rain and one with ice. Heavy rain causes both attenuation and depolarization. In some rain events, the attenuation and isolation vary independently in response to the rain rate. The isolation changes in response to both attenuation and depolarization. This will be called a rain attenuation/depolarization event. In other events, the cross-polarized signal remains approximately constant while the co-polarized component fades; changes in the attenuation are reflected directly in the isolation. This will be called a rain attenuation event.

The distinction between attenuation/depolarization events and attenuation events is usually unimportant in propagation research. However, the two kinds of events produce different correlation patterns, as this thesis will show.

The third type of event is ice-induced depolarization. This type of event is associated with cold fronts, where the ice depolarization occurs mainly above convective cells.

Ice depolarization also occurs during thunderstorms, but intense rain in the path will usually mask out any ice effects. For this reason, ice is usually noticed at the beginning or end of a thunderstorm. Attenuation levels during ice depolarization events are usually near zero and remain fairly constant. Thus, for the case of pure ice depolarization, any significant change in isolation is caused by the ice depolarization.

Each of the three types of events have unique expected correlation patterns. We will now discuss these expected patterns.

3.3.1 Ice-Induced Depolarization

The simplest case is that of ice depolarization. An ice-induced depolarization event (ice event) occurs without significant change in the co-polarized signal. The attenuation levels are normally close to zero while depolarization is significant. The attenuation is usually nearly constant as well as small, so the attenuation correlation coefficients are nearly zero. The isolation correlation coefficient can be either positive or negative. For example, if the isolation is decreasing with time, a positive coefficient would occur if backscatter from a range gate was decreasing with time. A negative coefficient would occur for

increasing backscatter from a range gate. Thus, for an ice event, the attenuation coefficients are nearly zero in each range gate and the isolation coefficients can be either negative or positive.

Another case of the ice depolarization event occurs when ice is present, along with significant rain. Thus, there is depolarization due to ice and attenuation/depolarization from the rain. This type of event contains significant depolarization, along with attenuation. Thus, the correlation pattern should not be as symmetrical as one from a rain-induced attenuation/depolarization event.

3.3.2 Rain Induced Depolarization and Attenuation

The problem is more complicated with rain. Attenuation and radar backscatter are both increasing functions of rain rate. But, isolation is the difference in dB between the co-polarized and cross-polarized signals, and its value is determined in a tradeoff between three things: the creation of the cross-polarized signal by the rain scatterers, the subsequent attenuation of the cross-polarized signal, and the attenuation of the co-polarized signal. Isolation and attenuation are usually related by [18]

$$I = U - V \log_{10}(A) \tag{3.1}$$

where V is usually equal to 20, A is the co-polarized signal level in dB, and I is the polarization isolation in dB. U and V are empirical and for the VPI&SU 11.6 GHz SIRIO system, they are 32.2 and 20 respectively. [19] U is a factor that depends on frequency, elevation angle and polarization. It is constant for a given path. It is obvious from this relationship that as the attenuation (A) increases, the isolation (I) decreases, and vice versa. Thus, the correlation coefficients for the two satellite signal quantities will have opposite signs. The attenuation coefficients can be either positive or negative, depending on the time dependence of the rain rate in the gate for which the coefficient is computed. Gates with the greatest rain rate should have high positive coefficients. The reason is that the attenuation, which is a lumped parameter, should be influenced more by gates with the highest rain rates. Thus, the attenuation and backscatter should track the rain rate and, in turn, track each other. Gates with less significant rain rate could be either positive or negative, depending on whether or not the rain rate (and, in turn, the backscatter) "track" the attenuation.

A rain attenuation (no depolarization) event occurs without significant fluctuation in the received cross-polarized signal. The cross-polarized signal stays approximately

constant while the co-polarized signal changes. This does not mean the cross-polarized signal stays at its clear weather value; it may be enhanced to a constant value for a small period of time. As previously stated, the change in attenuation is reflected exactly by the isolation since the cross-polarized signal is constant. The attenuation and the isolation differ by a constant; as the attenuation increases by a certain amount, the isolation decreases by the same amount. This is shown in equations (3.2) and (3.3).

$$\text{attenuation} = K_1 - CO \ (dB) \tag{3-2}$$

where K_1 is the clear weather co-polarized signal (a constant) and CO is the co-polar signal.

$$\text{isolation} = CO - K_2 + K_3 \ (dB) \tag{3-3}$$

where K_2 is the constant cross-polarized signal (for this case) and K_3 is the channel gain difference. As CO increases, attenuation decreases and isolation increases, and vice versa. For this special case the correlation plots will be exact mirror images. The correlation coefficient of the attenuation will always be the negative of the correlation coefficient of the isolation. This case does not occur often because the cross-polar signal is rarely constant for a varying co-polar signal.

The limiting cases that should be observed are (1) rain attenuation where changes in isolation are directly attributable to attenuation and (2) ice events, which have strong depolarization but very little attenuation. In Case 1 the attenuation and isolation correlation plots are exact mirror images. In Case 2 the attenuation correlation coefficients are small and the isolation correlations are high. They may be positive or negative. The third case, a rain-induced attenuation/depolarization event produces correlation plots that are between the two limits. These are not exact mirror images because of depolarization; changes in both the co-polarized satellite signal and the cross-polarized signal are reflected in the isolation.

Equation (3.1) describes rain propagation. Over any range of a values it may be approximated by a linear equation

$$I = C_1 + C_2(A) \tag{3.4}$$

where A is the co-polarized signal attenuation in dB, and C_1 and C_2 are coefficients whose value depends on the range of A considered. The smaller the range, the better the approximation. Equation (3.4) would lead to mirror-image correlation coefficients for I and A; hence the deviation of the correlation coefficients for mirror images is probably re-

lated to the amount of depolarization caused by ice above or mixed with the rain.

The three types of correlation plot patterns have been discussed. The first type of pattern had attenuation correlation coefficients that were approximately zero and isolation correlation coefficients that varied between positive and negative values. This pattern was related to ice-crystal depolarization. A combination of ice crystal depolarization and rain induced depolarization/attenuation was also discussed. This type of event should produce a correlation pattern that is between the approximate mirror image case of rain-induced attenuation/depolarization and the pattern for ice-crystal depolarization. The second type was nearly a mirror image and was related to the rain-induced attenuation/depolarization event. The third pattern was the exact mirror image plot. This pattern was a special case of the rain-induced attenuation/depolarization event. Examples of these three correlation patterns will be given in the next chapter.

Chapter IV

ANALYSIS OF REPRESENTATIVE EVENTS

The previous chapter discussed the type of events that may be observed and discussed their correlation patterns. This chapter presents data from representative events. The ice-induced depolarization event will be presented first. These will be followed by the rain-induced attenuation/depolarization events and a rain attenuation (no depolarization fluctuation) events.

4.1 ICE DEPOLARIZATION

An example of a correlation pattern for an ice-induced depolarization event, in which the attenuation coefficients are approximately zero, is taken from an event that occurred on 4 September, 1981. This ice event occurred during a light rain (rain rate at the main site reached a high of 1.44 mm/hr and a low of .97 mm/hr). The correlation pattern for this type of event, as previously discussed, should have attenuation coefficients near zero (due to the low and insignificant attenuation values) and isolation coefficients that vary, depending on the location of the scatterers causing the depolarization.

The correlation analysis was applied to the 4 September 1981 event for the time period of 13:54:30 to 14:02:20 GMT. The plot of the attenuation and isolation correlation coefficients for this period are shown in Figure 4-1. The pattern of the plot is as expected; the attenuation coefficients are near zero, while the isolation correlation coefficients are much higher. The significance probabilities of the attenuation coefficients were much higher than those for the isolation coefficients, suggesting the attenuation coefficients have a higher probability of arising from chance fluctuation in the data. Most of the probabilities were acceptable, still suggesting the attenuation coefficients are close to zero. The isolation coefficient plot is very interesting. The pattern has two very pronounced peak areas, one extending from gate 7 to 12 and the other extending from gate 15 to gate 30. The peak coefficient in the range from gate 7 to gate 12 is 0.84724 while the minimum is 0.5. The peak coefficient in the range from gate 15 to gate 30 is 0.84563 while the minimum is 0.5. The values of coefficients contained in these two ranges suggest the scatterers causing the depolarization are located in these two ranges.

The satellite signal attenuation and isolation are plotted vs. time in Fig. 4-2. The attenuation remains almost

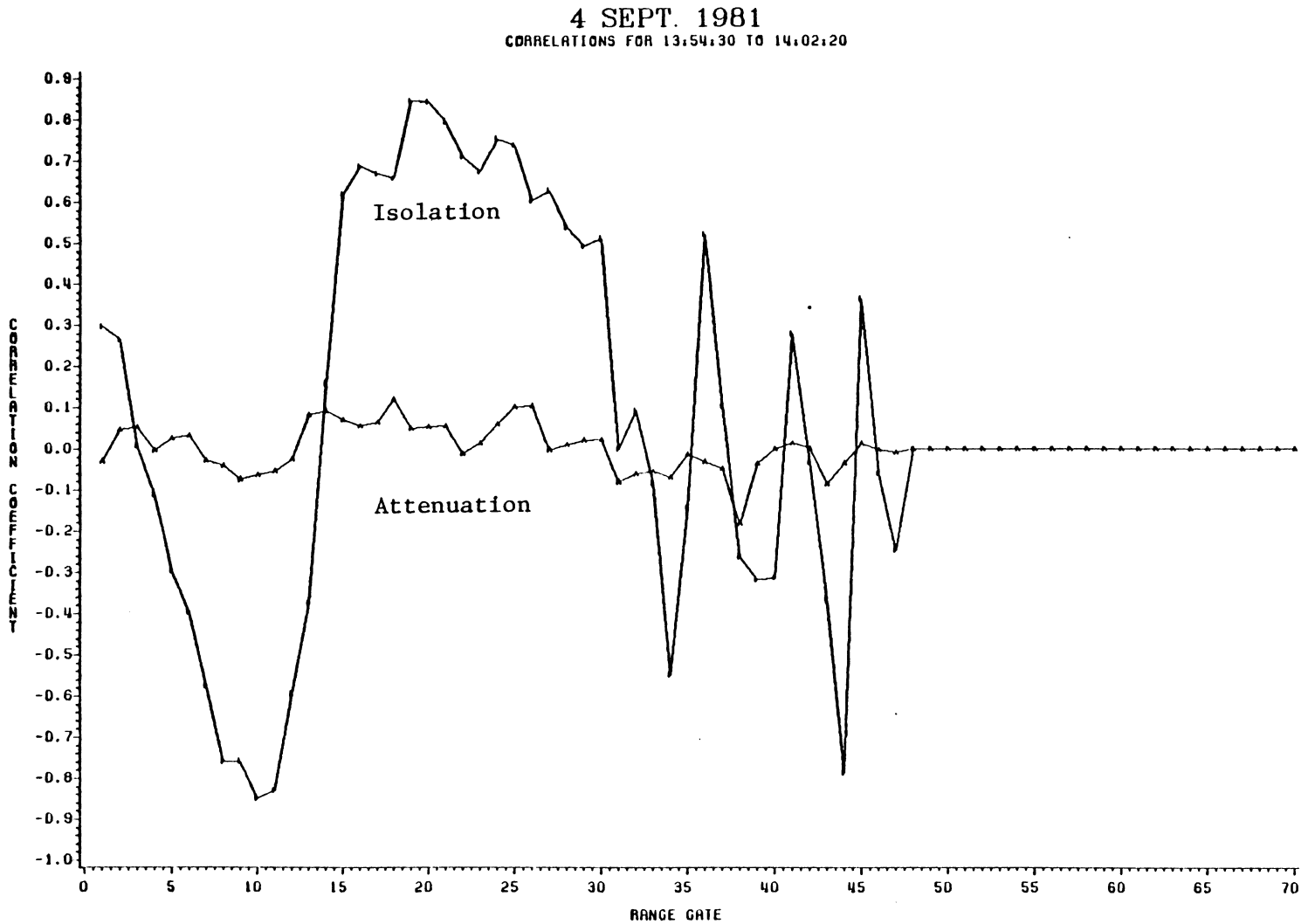

Figure 4-1. Correlation of isolation and attenuation with backscatter for the event of 4 September 1981.

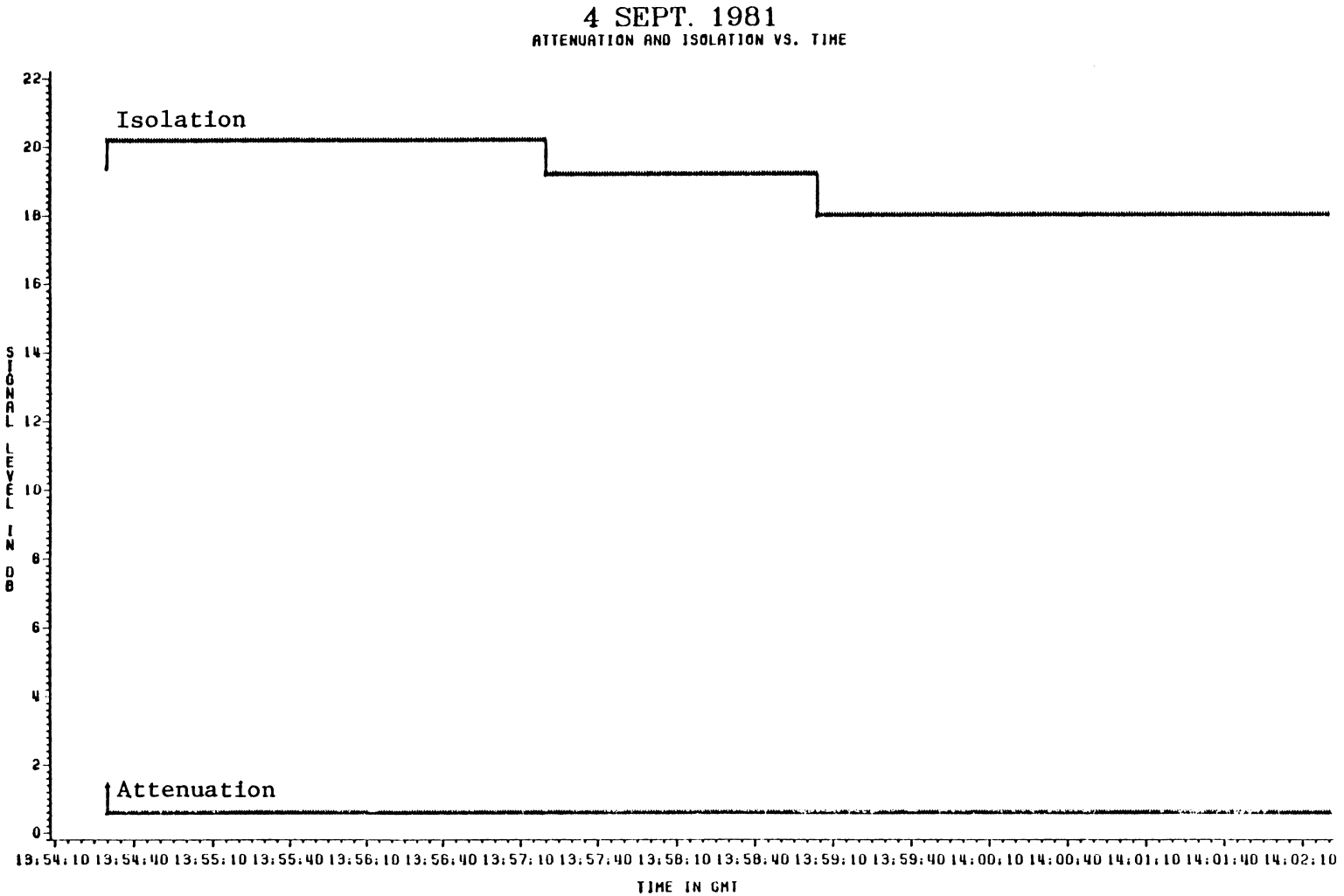

Figure 4-2. Attenuation and isolation vs. time for the event of 4 September 1981.

constant at 0.6 dB while the isolation decreases from 20.19 dB to 17.99 dB. The nearly constant attenuation and the changing isolation are characteristics of ice-crystal depolarization. The decrease in isolation, as displayed in Fig. 4-2, is slight, suggesting weak depolarization. This decrease in the isolation is not due to any changes in the satellite orbit or power output. This can be verified in Fig. 4-3, where the cross-polarized signal received at two separate stations. One is the system at the Virginia Tech Satellite Tracking Station (main site) and the other a station located 7.3 km from the main site. Differences in the absolute levels of the two signals are due to differences in receiver design and are not significant. As can be seen in Fig. 4-3, the cross-polarized signal received at the main site is increasing, while that received at the other site increases and then decreases. Any changes in the isolation displayed in Fig. 4-2 are not due to changes in the satellite orientation. The nearly constant attenuation and changing isolation suggest ice depolarization.

The coefficients contained in the two regions previously discussed suggest the backscatter from the range gates in these two regions tracks the isolation decrease. Backscatter from the first regions tracks the isolation in a negative sense, i.e. as the isolation decreases, the backscatter

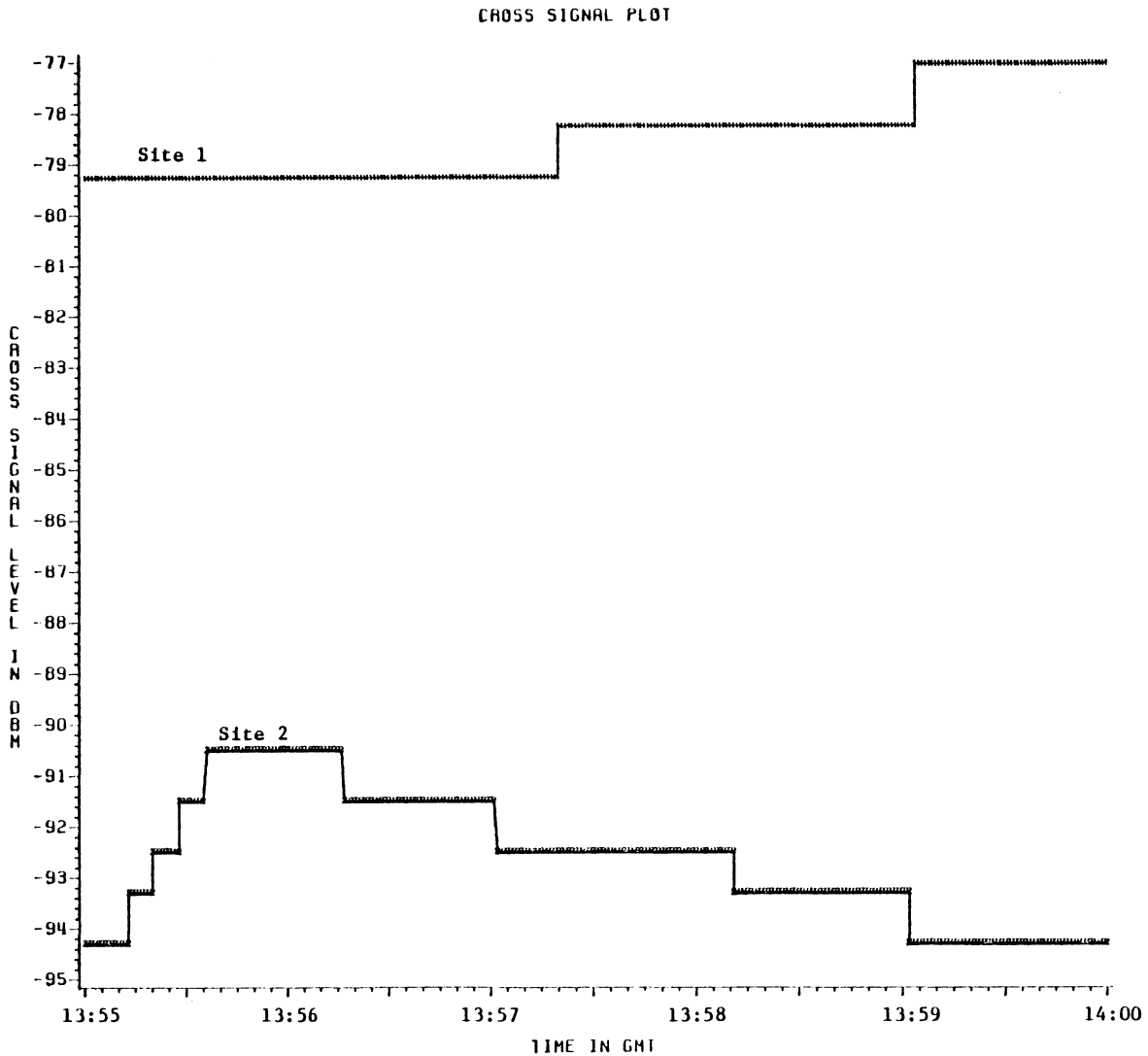

Figure 4-3. Cross-polarized signal level at the main site (1) and site (2) for the event on 4 September, 1981.

increases. The opposite is true for the second range, where the positive coefficients are located. The backscatter from these range gates tracks the isolation; as the isolation decreases, the backscatter from these gates also decreases. The backscatter from the two regions correlate well with the isolation decrease.

The strong correlations for the gates contained in the two regions discussed suggest the scatterers causing the depolarization are located in these two regions. However, other evidence suggests ice cannot be located below gate 35, corresponding to an elevation of 3.36 km. This is shown in Fig. 4-4 where range gates (1 gate = 500m), time in GMT, and radar backscatter in dBZ are plotted in a three-dimensional graph. An important characteristic of this plot is the peak in radar reflectivity around range gate 33. This is the "bright-band" region which is the melting layer associated with ice. Ice, which exists above the 0°C isotherm, falls below the isotherm and begins to melt. This melting region consists of water-coated particles which cause the bright band characteristic. Therefore, if ice exists, it must be beyond the bright band region, or roughly past gate 35. This range gate location also agrees well with temperature data.

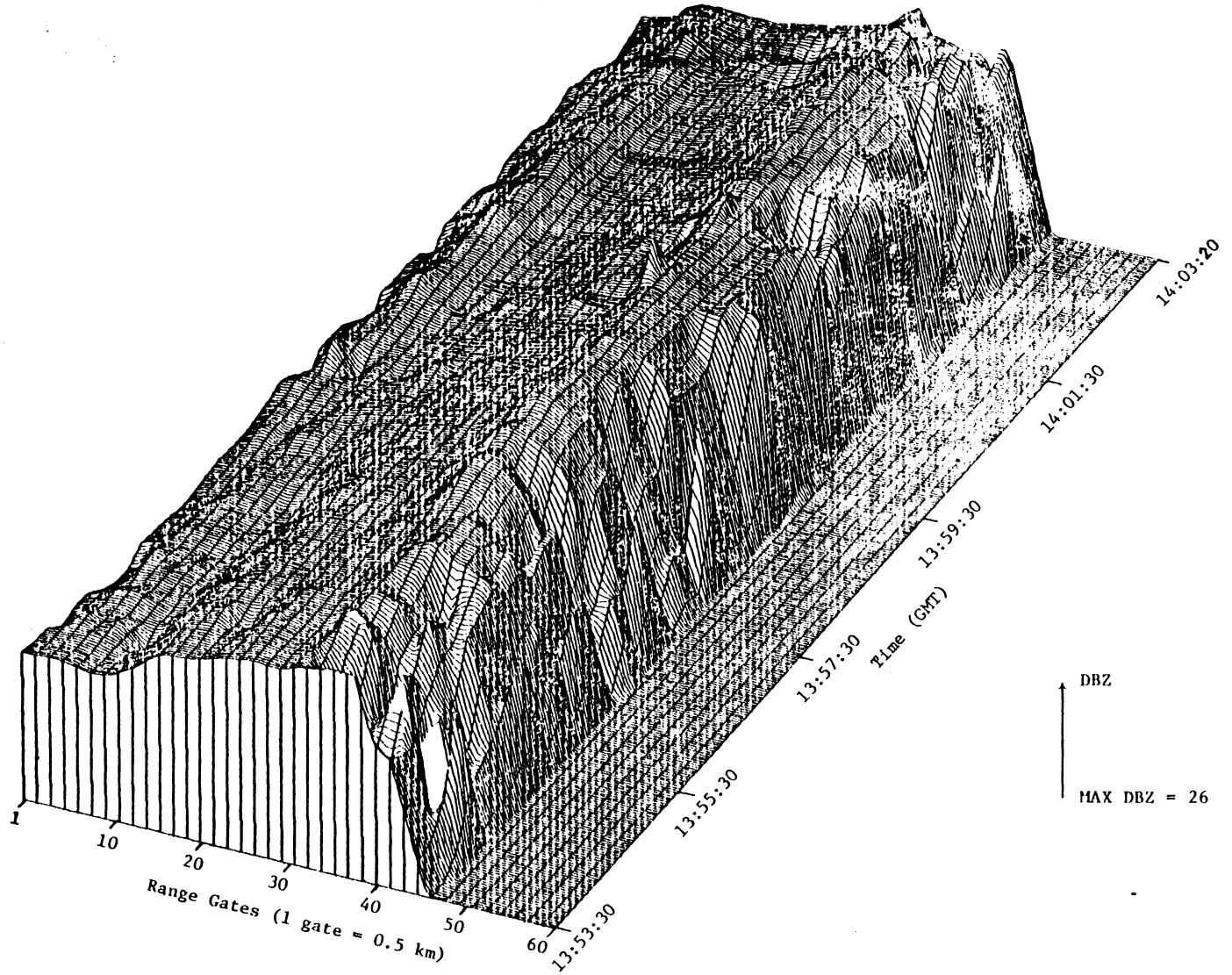

Figure 4-4. Three-dimensional plot of range gate, time and dBZ for the event of 4 September, 1981.

The temperature recorded in nearby Roanoke, VA at 8:30 AM (EST) on 4 September 1981 was 19°C [20]. Roanoke is approximately 1000 feet (0.3048 km) lower in elevation than Blacksburg. Gate 35 corresponds to an altitude of 3.36 km. Thus, gate 35 is approximately 3.6648 km higher in elevation than Roanoke. Assuming the temperature decreases at -5°C/km, the temperature at gate 35 is approximately 0.676°C. This suggest that 0°C isotherm exists roughly around gate 35, supporting the evidence of the bright band being around gate 33.

The two regions of good correlation, as previously discussed, suggest that ice exists in the range from gates 7 to 12 and gates 15 to 30. The elevation of these gates does not agree with the meteorological evidence; they are too low for ice to exist in them. For the case of ice depolarization, the isolation coefficients should indicate the gates containing the ice. However, the isolation did not decrease much (2.2 dB), suggesting weak depolarization. More severe ice depolarization may be needed for the correlation analysis to detect the location of the ice, i.e. more ice may be needed in the path.

The first region of strong correlation coefficients (gates 7 to 12) suggests the time variation of the scatterers in these gates tracks the isolation time variation in a

negative sense. However, it should be pointed out that radar return from the region around range gate 10 is often contaminated with ground clutter. This comes from the peak in the range gate 10 area. This peak can be seen in Fig. 4-5, where a flat earth terrain profile of a section of the propagation path is shown. This first peak is labeled A. The increasing backscatter from the gate 10 area can be seen in the three-dimensional plot of Fig. 4-4. The backscatter from this area starts increasing at the halfway point on the time axis. It is uncertain whether or not this is due to clutter.

The second region of correlation coefficients (gates 15 to 30) suggests the radar backscatter from these gates has the same time variation as the isolation (in a positive sense). Again, the problem of ground clutter exists; the region around gate 20 is often contaminated. The source of the ground clutter is the region around the peak labeled B. Because the isolation correlation coefficients are relatively high beyond the gate 20 area, it is unlikely this second region (gates 15 to 30) is influenced greatly by ground clutter. Though the correlation coefficients in the second region (gates 15 to 30) do not represent ice (discussed previously), they probably do represent the backscatter from some hydrometeor (rain) and are not due to ground clutter.

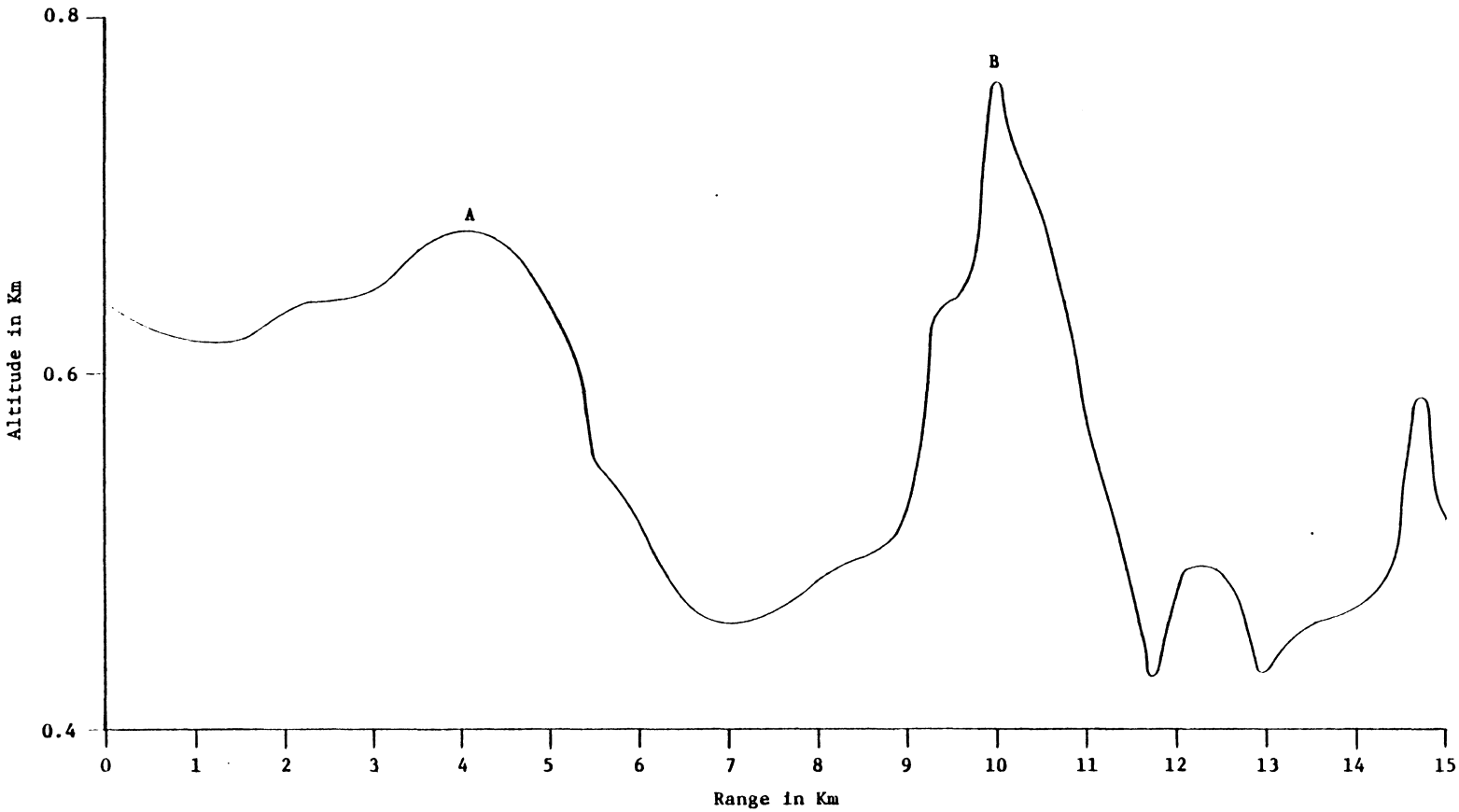

Figure 4-5. Terrain profile for a section of the propagation path (azimuth = 105.8°). Each km is approximately 2 slant path range gates.

The fluctuating isolation coefficients in the outer gates are due to the noise floor of the radar system.

The correlation plot presented for the 4 September 1981 event is the expected pattern for an ice-induced depolarization event. Though the correlation coefficients in the two regions discussed (gates 7 through 12 and gates 15 through 30) do not represent ice, the correlation pattern is still what is expected. In this example, the correlation technique did not correctly locate the ice causing the depolarization. The major problem associated with this particular event is that the ice depolarization is weak. Perhaps if greater ice concentrations existed, the correlation analysis could be used to detect the ice location. It is also possible the region beyond the gate 20 area is filled with wet snow, which would cause the depolarization. If this is the case, the correlation plot Fig. (4.11) indicates the location of the wet snow. Again, this is only a possibility.

The next correlation pattern to be discussed is an example of rain-induced attenuation/depolarization occurring with another form of depolarization. The event occurred on 27 October 1981. Because another form of depolarization (possibly ice-induced) occurs along with the rain-induced attenuation and depolarization, the expected correlation pattern should not be as symmetrical as the pattern obtained

from a rain-induced attenuation/depolarization event. The correlation analysis was applied to this event for the time period 01:35:00 to 01:55:00 GMT. The plot of the attenuation and isolation correlation coefficients is shown in Fig. 4-7. The correlation pattern is not as symmetrical as one displaying attenuation and isolation coefficients for a rain-induced attenuation/depolarization event (for example, the coefficient plot for the 22 September 1980 event in Fig. 4-9). This is to be expected.

For a rain event such as the one occurring on 22 September 1980, the range of attenuation limits the I = U - V log(A) relationship to a nearly-linear portion of the curve. Though the attenuation and isolation appear to be linearly related in the plot (Fig. 4-10), they actually are not. This was discussed previously. If there is significantly more depolarization present than the rain produced (possibly caused by ice), the correlation pattern should not be as symmetrical as one for a rain induced attenuation/depolarization event. This is the case for the correlation plot in Fig. 4-6, suggesting another depolarizing agent is present.

The satellite signal attenuation and isolation are plotted in Fig. 4-7. This plot is not as symmetrical as a similar plot for a rain-induced attenuation/depolarization event, such as the one 22 September 1980. The attenuation

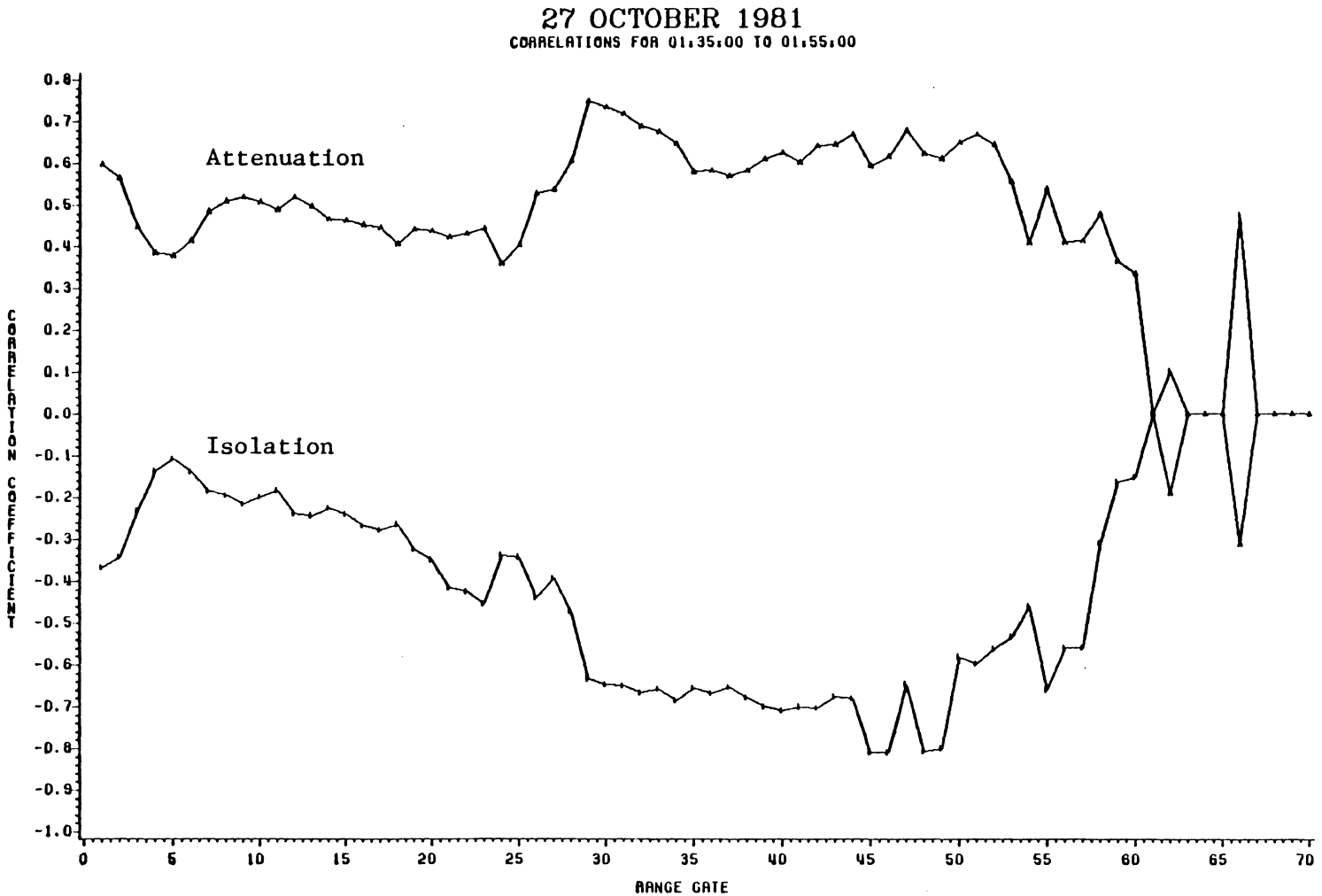

Figure 4-6. Correlation of isolation and attenuation with backscatter for the event of 27 October 1981.

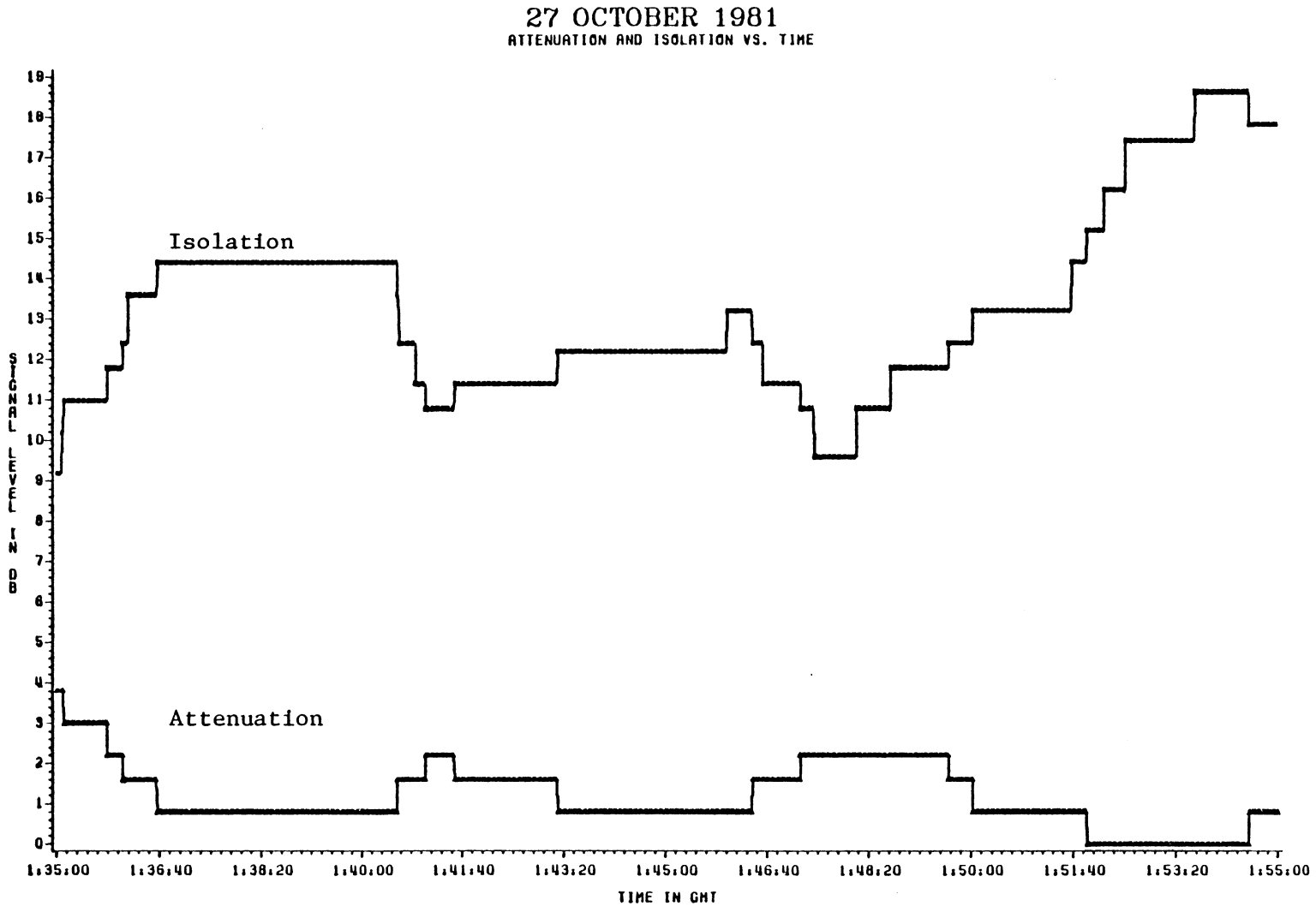

Figure 4-7. Attenuation and isolation vs. time for the event of 27 October 1981.

change does not always correspond to an approximately similar change in isolation. An important characteristic of the plot in Fig. 4-7 is the low values of isolation observed through most of the period. These low values of isolation, along with relatively low values of attenuation, suggest ice depolarization. However, ice depolarization is normally associated with lower and more constant attenuation levels than those observed here. The attenuation/depolarization may be due to wet snow. This is consistent with the data being observed. The melting snow could form rain that would attenuate, while the wet snow itself could induce depolarization. From the observations made, this is probably the type of event that occurred. Further evidence of another depolarizing agent (probably wet snow) exists.

Shown in Fig. 4-8 is a three-dimensional plot showing time, range gate and radar backscatter along the X, Y and Z axes respectively. The most outstanding feature of this is the peak around range gates 27 to 33. This peak represents the bright band region. Though the bright band is normally associated with ice which falls below the 0° isotherm and melts, it also occurs with the wet snow event. [21] For the case of ice, the ice particles fall below the 0°C isotherm and begin to melt, thus causing the bright band region. As this melting ice falls, it forms a light rain which causes

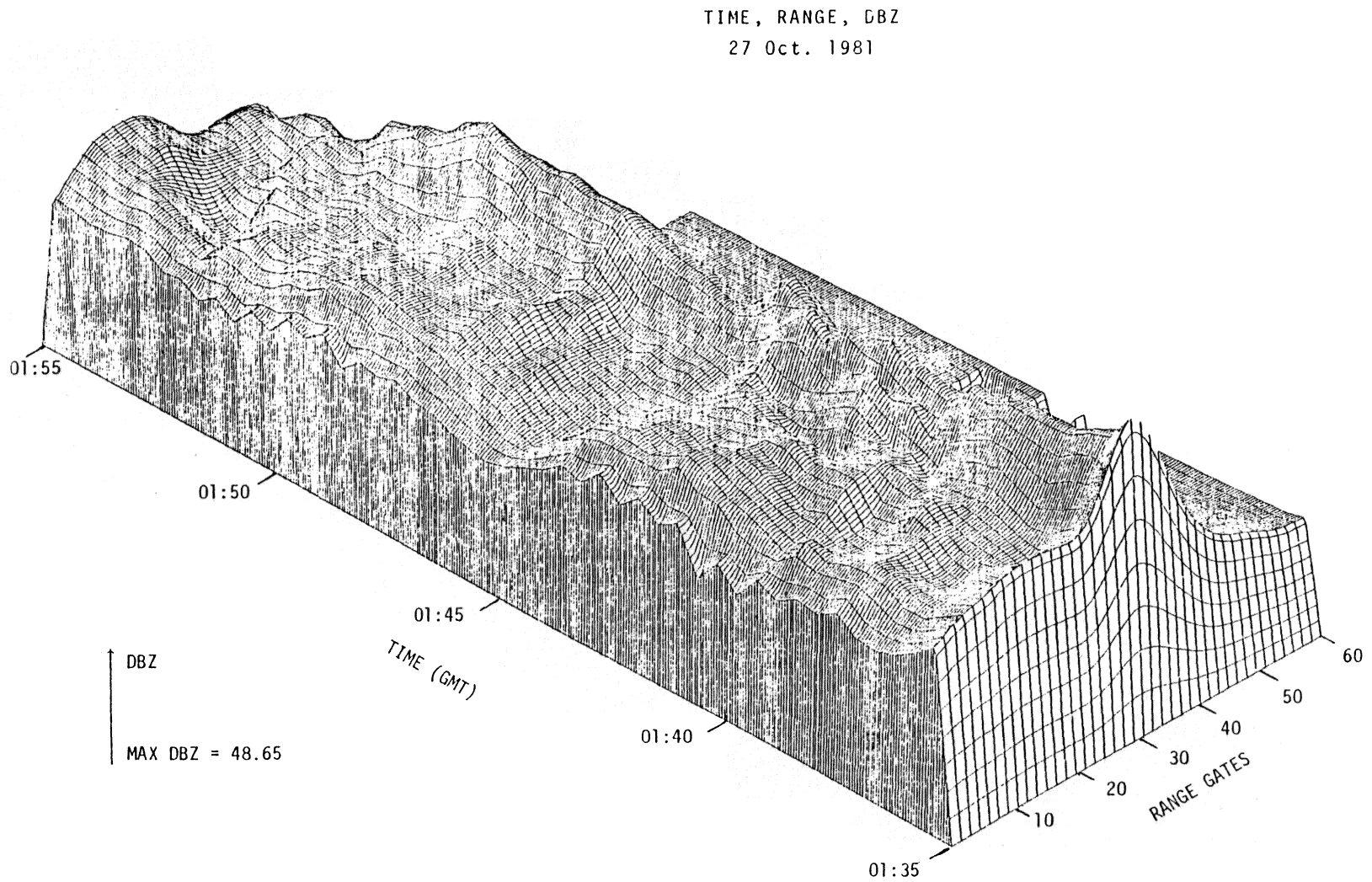

Figure 4-8. Three-dimensional plot of range gate (1 gate = 500m), time and dBZ for the event of 27 October 1981.

near-zero attenuation levels. For the case of wet snow, snow falls below the 0° isotherm and begins to melt. This wet snow, which causes depolarization, also forms the bright band region. As the melting snow continues to fall, rain is formed. This rain causes significant attenuation.

Another interesting characteristic of the three-dimensional plot in Fig. 4-8 is the backscatter from the bright band starts decreasing at approximately 01:51:30 GMT. This compares very well with the increase in isolation that occurs at approximately 01:51:00. This decrease in the isolation associated with the decrease in backscatter from the bright band suggests the depolarizing agent was located in the bright band region. This would be the case for the wet snow event, where the depolarizing agent is wet snow and is located in the bright band region.

This event is a good example of a combination of rain-induced attenuation/depolarization occurring with another depolarizing agent, in this case, probably wet snow. This type of event gives rise to the non-symmetrical attenuation and isolation coefficient patterns.

4.2 RAIN-INDUCED ATTENUATION/DEPOLARIZATION

An example of a rain induced depolarization/attenuation correlation pattern is taken from an event that occured on 22 September, 1980. This was a fade event with slight depolarization. For this reason, the expected correlation pattern is nearly a mirror image. The correlation analysis was done for the time period of 18:17:00 to 18:22:00 GMT and the results are plotted in Fig. 4-9. The correlation coefficients are almost, but not quite, mirror images.

An interesting characteristic of the correlation plot in Fig. 4-9 is that most of the attenuation coefficients are high positive values, with the exception of two gates. The negative attenuation correlation coefficient of gate 1 is not impossible; the attenuation, which is a function of the integrated rain rate along the propagation path, may be decreasing with time while the backscatter from a gate is increasing with time. Ground clutter may be the cause of the negative coefficient in gate 1. The rapid fluctuation at gate 10, which is not consistent with the other coefficients, is possibly due to ground clutter. As previously discussed the gate 10 area is often contaminated with ground clutter, due to the increasing terrain elevation under the gate 10 area. The correlation coefficients are zero past gate 19 because no significant signal was received from the gates after 19.

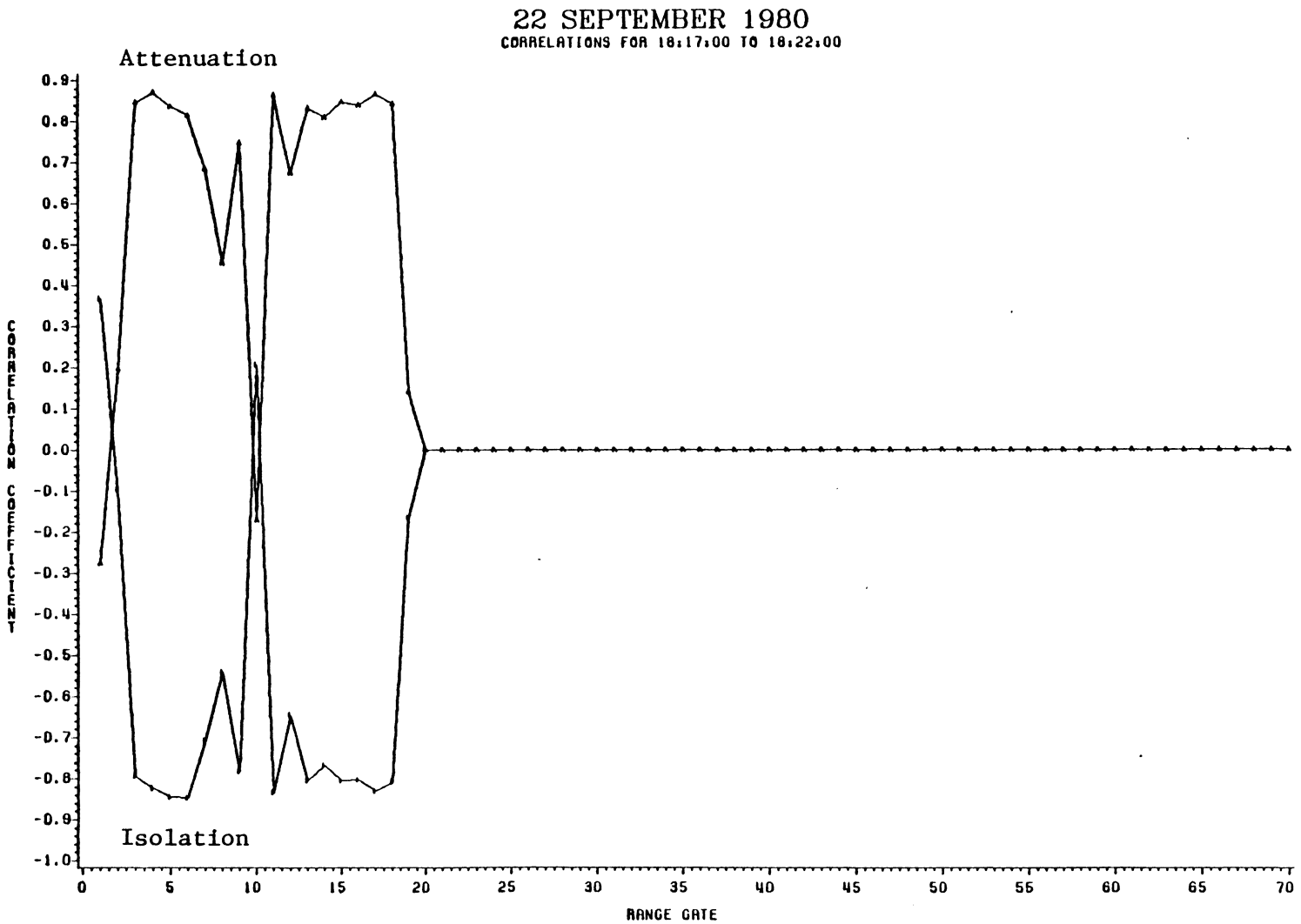

Figure 4-9. Correlation of isolation and attenuation with backscatter for the event of 22 September 1980.

The satellite signal isolation and attenuation plots for the time period from 18:17:00 to 18:22:00 GMT are shown in Fig. 4-10. Because the correlation patterns are nearly mirror images of each other, the attenuation and isolation plots are expected to be nearly mirror images of each other. Departure from the mirror image behavior occurs when both the co- and cross-polarized signal components change simultaneously. Mirror images result when the cross-polarized signal remains constant and the co-polarized component varies.

This is an expected result; we will show that mirror image behavior is predicted from equation (3-1). For the Virginia Tech 11.6 GHz SIRIO system, the constants U and V are empirically 32.2 and 20, respectively. [19] However for the range of attenuation observed in this event, (approximately 3 to 12 dB), the I-A relationships can be approximated well by a straight line. This approximation gives a maximum error of about 2 dB. This is shown in Fig. 4-11, where the bounds on I and A are taken from the isolation and attenuation plot in Fig. 4-10. Though the attenuation and isolation plot shown in Fig. 4-10 appears not to follow the non-linear I-A relationship, it actually does; the slight non-linearity does not stand out in the plot.

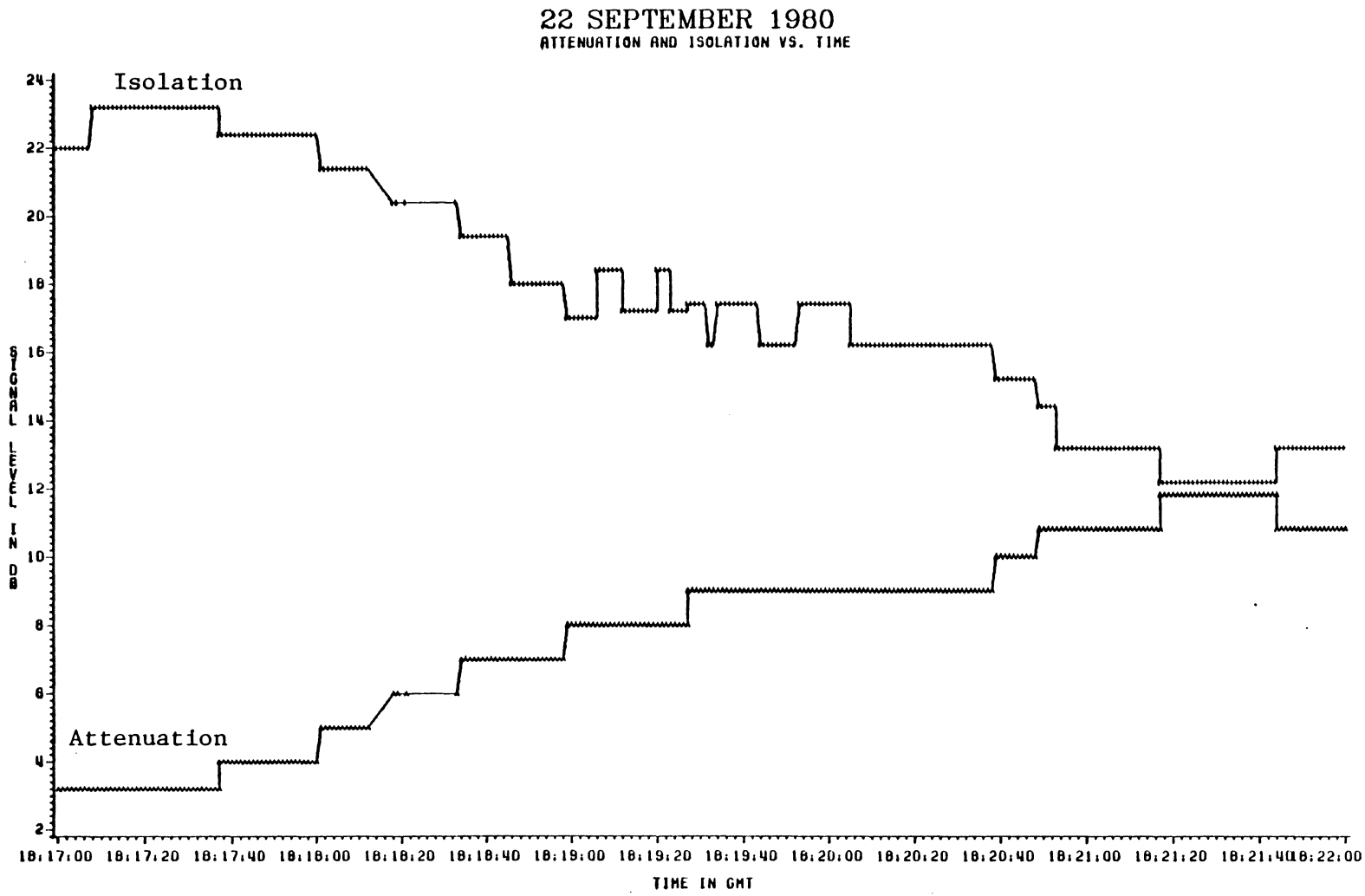

Figure 4-10. Attenuation and isolation vs. time for the event of 22 September 1980.

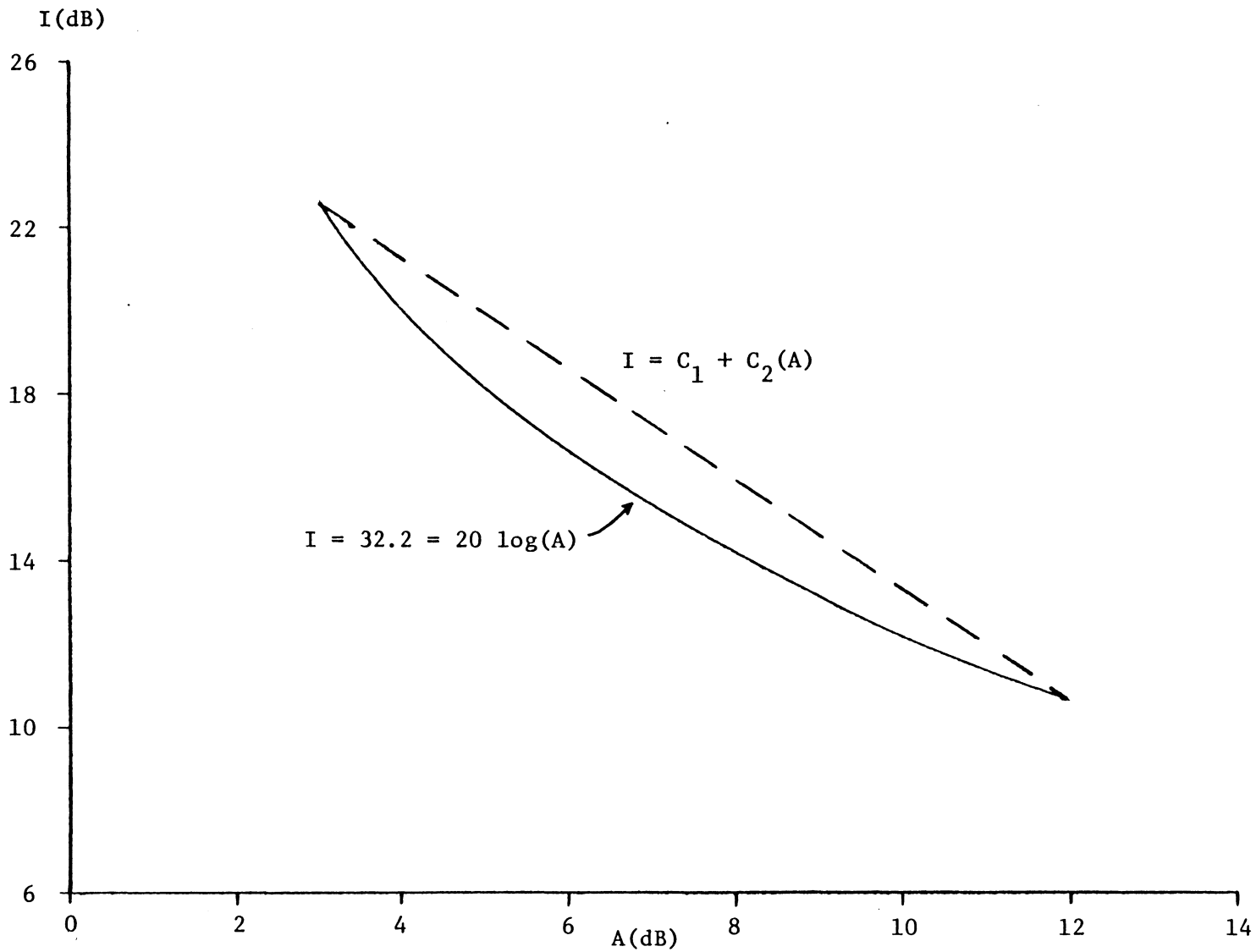

Figure 4-11. Isolation and attenuation using I = 32.2 - 20 log(A) and I = C_1 + C_2(A).

The high positive attenuation correlation coefficients indicate that the attenuation "tracks" the radar backscatter. From the correlation plot (Fig. 4-9), the maximum attenuation correlation coefficient (0.86386, significance probability = 0.0001) occurs in gate 11. This high coefficient indicates the attenuation closely tracks the radar backscatter. This is also evident from Fig. 4-12 where satellite signal attenuation and isolation and radar backscatter are plotted versus time.

This event contains a good example of the correlation pattern expected from a rain induced depolarization/attenuation event. The near mirror image pattern is typical.

An example of a pure fade event correlation pattern is taken from an event that occured on 30 August 1981. This is characterized as a pure fade event because the depolarization does not fluctuate and all changes in the attenuation are reflected directly in the isolation. Thus, as the attenuation increases, the isolation decreases and vice versa. This does not imply depolarization is not present, only that it remains approximately constant over a period of time. This is due to the cross-polarized signal not changing by more than 0.7 dB, which is the change necessary for a signal level to be recorded.

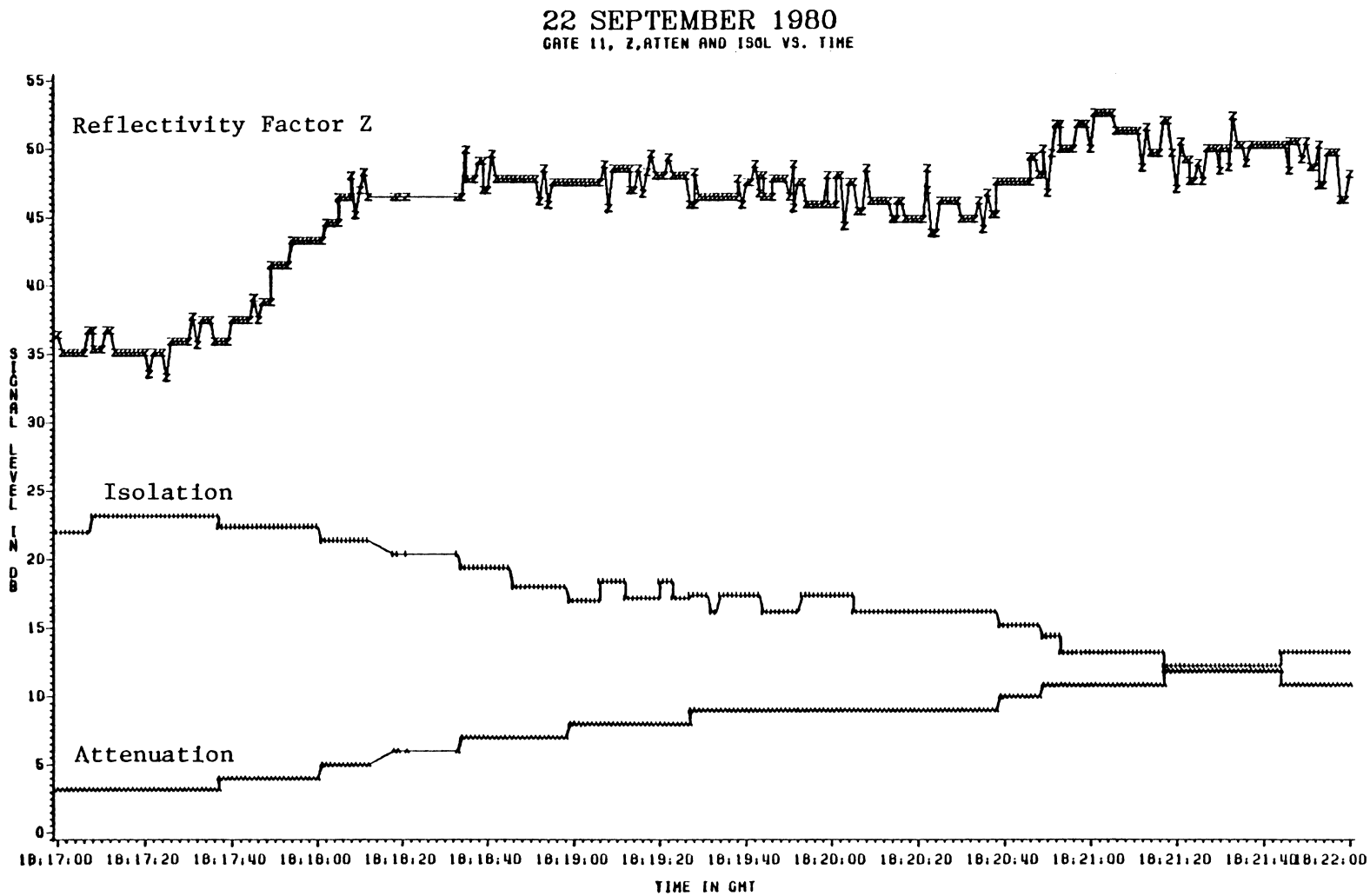

Figure 4-12. Attenuation, isolation and radar reflectivity factor vs. time for Gate 11.

Because the attenuation changes are the only changes in the isolation, the correlation coefficient patterns of the isolation and attenuation should be exact mirror images of each other. The correlation analysis was performed on the 30 August 1981 event for the time period of 23:33:00 to 23:38:00 GMT. The plot of the isolation and attenuation correlation coefficients is shown in Fig. 4-13. The patterns of the isolation and attenuation coefficients are mirror images of each other. The coefficients are fairly stable past gate 21, i.e. they do not fluctuate a lot from gate to gate. Most of the attenuation coefficients are high positive values between gates 20 and 36. This suggests the attenuation changes in the same direction as the radar backscatter. Without meteorological information, which is not available, it is difficult to determine exactly what is happening from gate to gate.

The satellite signal attenuation and isolation are plotted versus time in Fig. 4-14. The attenuation increases with time from 9.0 dB to 12.6 dB an overall change of 3.6 dB. The isolation decreases from 10.38 dB to 6.78 dB, an overall change of 3.6 dB, the same as that of the attenuation. This is expected because the isolation and attenuation change the same amount each time, only in opposite directions. Though only attenuation changes are present, the

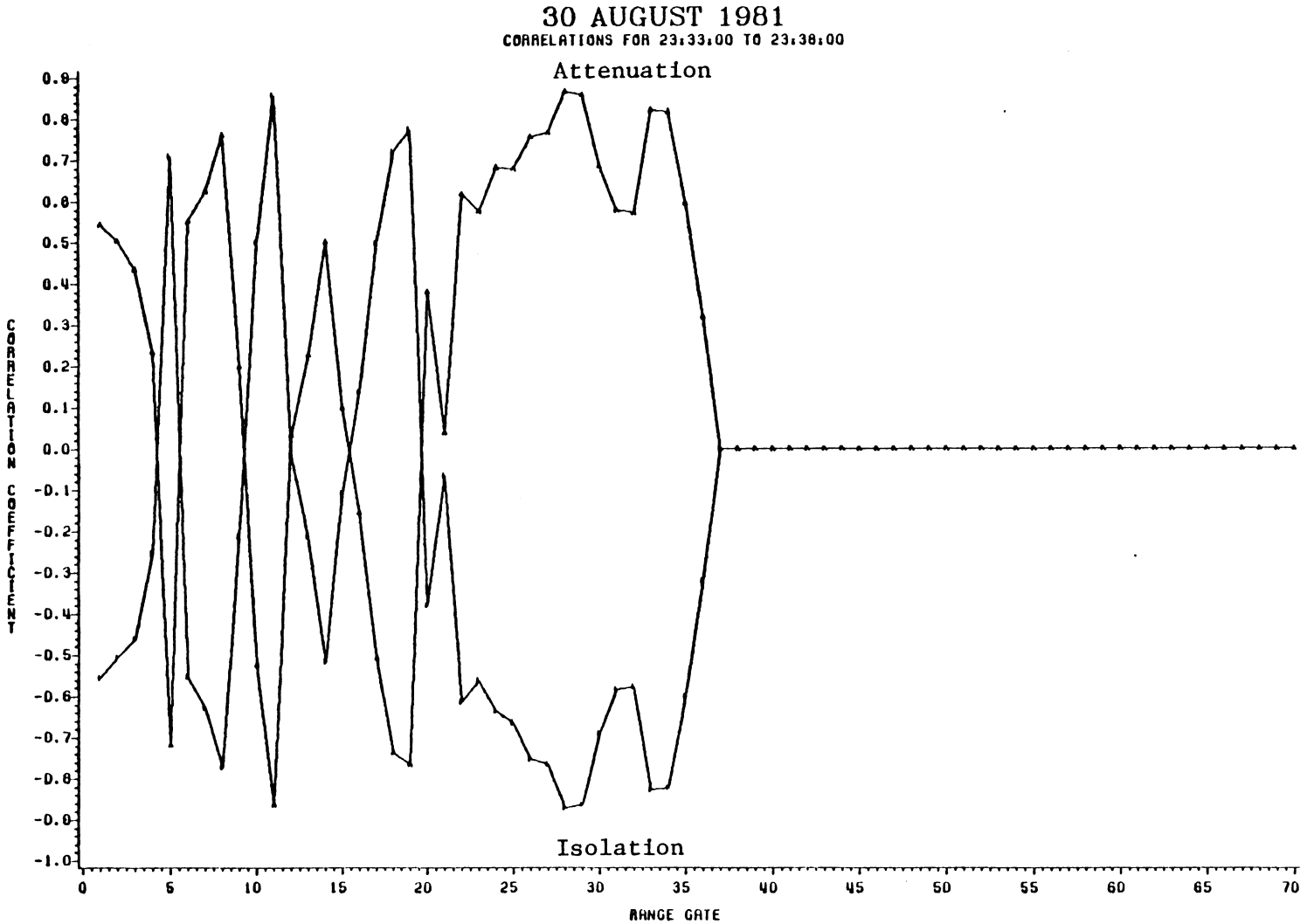

Figure 4-13. Correlation of isolation and attenuation with backscatter for the event of 30 August 1981.

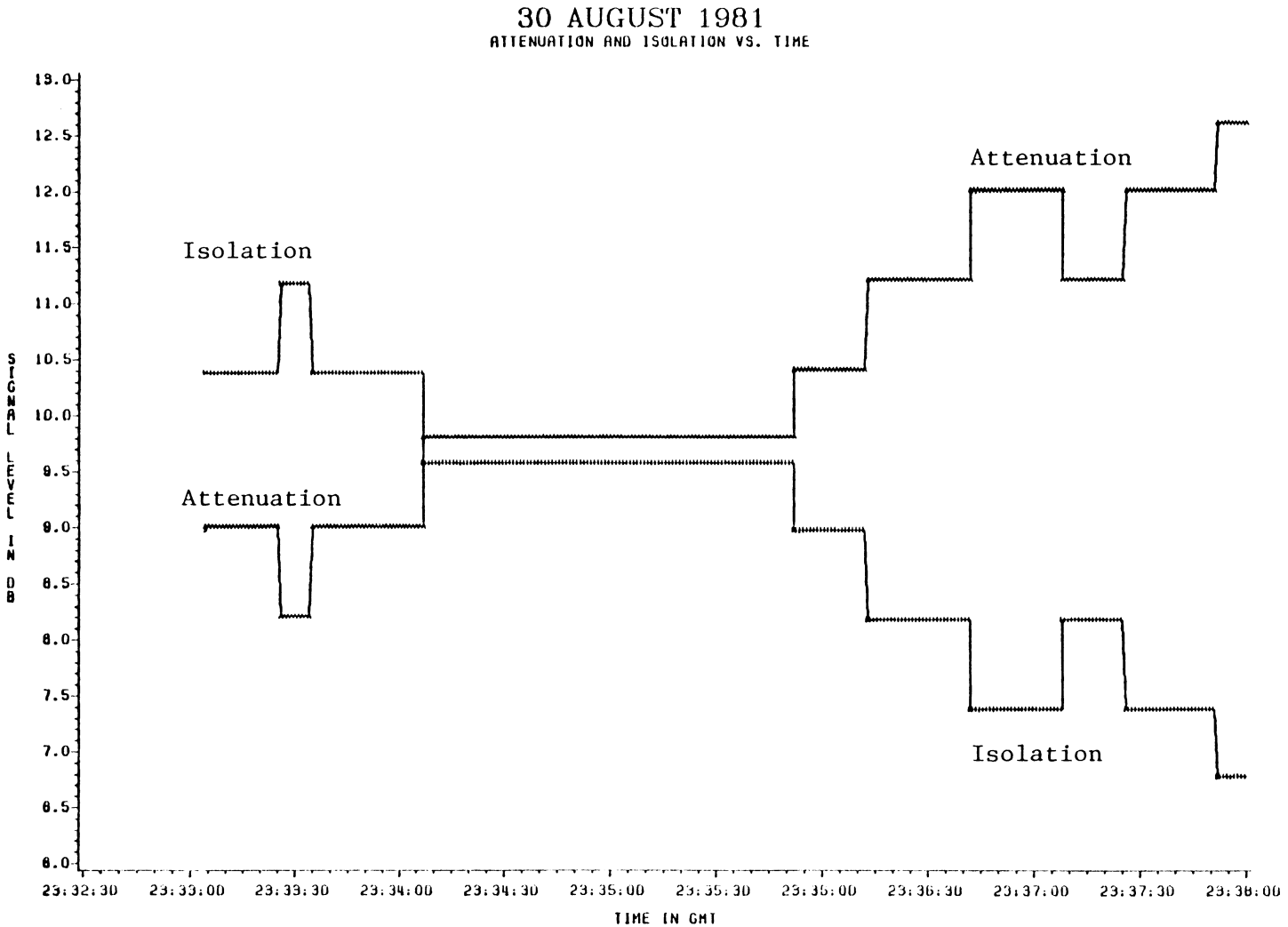

Figure 4-14. Attenuation and isolation vs. time for the event of 30 August 1981.

low value of isolation (10.38 dB) indicates that depolarization is present. This is actually a special case of the rain-induced fade/depolarization pattern previously discussed.

The events that have been discussed are examples of the types of correlation patterns that are expected for various types of attenuation and isolation activity. These have demonstrated that the degree to which the patterns are mirror images depends on the type of depolarization activity present. Ice-induced depolarization produces one of two different patterns, depending on whether or not rain-induced depolarization/attenuation is also present. Rain-induced depolarization/attenuation produces a pattern that is very symmetrical. The perfect mirror image is actually a special case of the rain-induced attenuation/depolarization event pattern.

Chapter V

SUMMARY AND CONCLUSIONS

This thesis examined the use of statistical correlation as a tool in propagation studies. This effort was an extension of the work published by Shutie, Allnutt and Mackenzie in 1977. [3] Their work used statistical correlation to determine the location of ice crystals causing depolarization, whereas this thesis extended statistical correlation to determine the type of event being observed.

The statistical correlation technique presented in this thesis was performed using the Pearson product-moment method. In this work, satellite signal attenuation and isolation (both in dB) were correlated with radar backscatter (dBZ) from each radar range gate. To check each coefficient for statistical significance, a significance probability was also computed using the t test. This is the probability due to a chance fluctuation in the data and is used to determine if the correlation coefficient is statistically significant. When the attenuation and isolation coefficients for the radar gates (out to range gate 70) are plotted, a certain pattern, which depends on the type of event being examined, is obtained. Thus, the pattern obtained from the coefficient plots can be used to distinguish the type of event.

Three distinct patterns are expected, each related to a certain type of event. An ice depolarization event should produce attenuation correlation coefficients that are equal to or near zero, due to the insignificant fade of the co-polarized signal. The isolation coefficient should vary from region to region along the path, depending on how the backscatter from each gate varies with time as compared to the time variation of the isolation. A rain attenuation/depolarization event should produce an attenuation coefficient pattern that is nearly a mirror image of the isolation coefficient pattern, i.e. the attenuation and isolation coefficients should have opposite signs but nearly equal magnitudes. This is due to the attenuation (A) and isolation (I) being related (for rain) by the $I = U - V \log(A)$ relationship; as A increases, I decreases and vice versa. The attenuation (or isolation) coefficients can be either positive or negative, depending on the time variation of the attenuation (or isolation) as compared to that of the radar backscatter from each gate. A rain attenuation event (no significant depolarization fluctuation) should produce attenuation and isolation coefficient patterns that are exact mirror images of each other. In this type of event, the cross-polarized signal remains at a nearly constant level (not necessarily the clear-weather values); any changes in

the attenuation are reflected directly in the isolation. The attenuation and isolation coefficients can be either positive or negative, as discussed previously for the rain attenuation/depolarization case. This rain attenuation case is actually a special case of the rain attenuation/depolarization case. This special case of rain attenuation and the case of ice depolarization are the limiting cases. It is possible to have an attenuation and depolarization event that does not obey the $I = U - V \log(A)$ relationship; more depolarization is present than this relationship suggests. For this type of event, the attenuation and isolation coefficient patterns should not be symmetric. The degree of asymmetry depends on the degree of depolarization and attenuation. Again, the attenuation and isolation coefficients can be either positive or negative. Examples of each of the events previously described have been presented. In each case, the correlation pattern obtained was the expected one. Though the pattern from the ice event of 4 September, 1981 did not indicate the location of the ice, the pattern obtained was the expected pattern.

This thesis has extended the work of Shutie, Allnutt and Mackenzie. The statistical correlation technique has been successfully used to determine the type of event being examined. Though the correlation technique was applied to re-

corded data, it may also be applicable to real time data and could be used to determine the type of event being observed with the radar and propagation link.

REFERENCES

1. J. Goldhirsh, "Ice Depolarization of the COMSTAR Beacon at 28.56 GHz During Low Fades and Correlation with Radar Backscatter," IEEE Transactions on Antennas and Propagation, Vol. AP-30, pp. 183-190, March 1982.

2. R. E. Marshall, E. A. Manus, P. H. Wiley and C. W. Bostian, "An S Band Radar for Studying the Effects of Weather on the SIRIO and COMSTAR Satellite Downlink Signals," 20th Conference on Radar Meteorology, 30 November - 3 December, 1981, Boston, Mass., American Meteorological Society, pp. 498-501.

3. P. F. Shutie, J. E. Allnutt, E. G. Mackenzie, "Satellite-Earth Signal Depolarization at 30 GHz in the Absence of Significant Fading," Electronics Letters, Vol. 13, pp. 1-2, January, 1977.

4. J. Goldhirsh, "Comparison of Radar Derive Slant Path Rain Attenuation with the COMSTAR Beacon Fades at 28.56 GHz for Summer and Winter Periods," IEEE Transactions on Antennas and Propagation, Vol. AP-28, pp. 577-580, July 1980.

5. M. P. M. Hall, S. M. Cherry, J. W. F. Goddard and G. R. Kennedy, "Rain Drop Sizes and Rainfall Rate Measured by Dual-Polarization Radar," Nature, Vol. 285, pp. 195-198, 22, May, 1980.

6. G. C. McCormick and A. Hendry, "Principles for the Radar Determination of the Polarization Properties of Precipitation," Radio Science, Vol. 10, pp. 421-434, April 1975.

7. A. Hendry, Y. M. M. Antar, J. J. Schlesak and R. L. Olsen, "Melting Layer Attenuation at 28.56 GHz from Simultaneous COMSTAR Beacon and 16.5 GHz Polarization Diversity Radar Observations," International Conference on Antennas and Propagation, Part 2, IEE Conference Publication No. 195, pp. 12-16, April 1981.

8. J. W. F. Goddard, S. M. Cherry and M. P. M. Hall, "Modeling Attenuation on an Earth-Space Path Using Dual-Polarisation Radar," International Conference on Antennas and Propagation, Part 2, IEE Confrence Publication No. 195,pp. 17-21, April 1981.

9. T. A. Seliga, V. N. Bringi, and H. H. Al-Khatib, "A Preliminary Study of Comparative Measurements of Rainfall Rate Using the Differential Reflectivity Radar Technique and a Raingauge Network," Journal of Applied Meteorology, Vol. 20, pp. 1362-1368, November 1981.

10. G. C. Towner, et al., "Initial Results from the VPI&SU SIRIO Diversity Experiment, Radio science, To be published in a 1983 special issue.

11. W. S. Burdic, Radar Signal Analysis, Prentice-Hall, Englewood Cliffs, N.J., 1968.

12. SAS Institute Inc. SAS User's Guide, 1979 Edition, Cary, NC, SAS Institute Inc., 1979.

13. A. Papoulis, Probability, Random Variables, and Stochastic Processes, McGraw-Hill, NY, 1965.

14. F. G. Stremler, Introduction to Communication Systems, Addison-Wesley, Reading, Mass., 1977.

15. C. C. Peters and W. R. Van Vooris, Statistical Procedures and Their Mathematical Bases, McGraw-Hill, NY, 1940.

16. J. S. Bendat and A. G. Piersol, Random Data: Analysis and Measurement Procedures, John Wiley and Sons, NY, 1971.

17. A. L. Edwards, Statistical Methods, Third Ed., Holt, Rinehart and Winston, NY, 1973.

18. L. J. Ippolito, "Radio Propagation for Space Communications Systems," Proceedings of the IEEE, vol. 69, pp. 697-727, June 1981.

19. M. P. M. Hall, Effect of the Troposphere on Radio Communications, Institute of Electrical Engineers, London, 1979.

20. "Weather Report", Roanoke Times and World Report, pp. A-6, September 5, 1981.

21. A. Hendry and Y. M. M. Antar, "Ice Crystal Observations at 1.8 cm Wavelength Using a Polarization Diversity Radar," 20th Conference on Radar Meteorology, Boston, November 30 - December 3, 1981, American Meteorological Society, pp. 579-585.

22. D. C. Hogg and Ta-Shing Chu, "The Role of Rain in Satellite Communications," Proceeding of the IEEE, vol. 63, pp. 1308-1331, September 1975.

23. R. R. Taur, Rain Depolarization: Theory and Experiment," Comsat Technical Review, vol. 4, no. 1, pp. 187-190, Spring, 1974.

24. T. Oguchi, "Attenuation of Electromagnetic Waves Due to Rain with Distorted Raindrops," Journal of Radio Research Lab., vol. 7, no. 33, September 1960.

25. J. Goldhirsh, "Correlation of Slant Path Ice Depolarization Events at 18.56 GHz with Radar Reflectivity Structure and the Determination of Ice Depolarization Statistics for Wallops Island, Virginia," International Conference on Propagation and Antennas, Part 2, IEE Conference Publication No. 195, April 1981.

26. P. F. Shutie, J. E. Allnutt and E. C. Mackenzie, "Satellite-Earth Signal Depolarisation at 30 GHz in the Absence of Significant Fading," Electronics Letters, vol. 13, no. 1, pp. 1-2, January 1977.

27. C. W. Bostian, et al., "Depolarization Measurements on the ATS-6 20 GHz Downlink," IEEE Transactions on Microwave Theory and Technique, vol. MTT23, pp. 1049-1053, 1975.

28. P. F. Shutie, E. C. Mackenzie and J. E. Allnutt, "Relative Phase Measurements Between Co-polar and Induced Cross-polar Signals Produced by Ice Particles on a Satellite-to-Ground Link, Electronics Letters, vol. 13, pp. 105-107, 1978.

29. D. C. Cox, H. W. Arnold and A. J. Rustako, Jr., "Some Observations of Anomalous Depolarization on 19 and 12 GHz Earth-Space Propagation Paths," Radio Science, vol. 12, no. 3, pp. 435-400, May-June 1977.

30. D. C. Cox, H. W. Arnold and H. H. Hoffman, "Depolarization of 19 and 28 GHz Earth-Space Signals by Ice Particles," Radio Science, vol. 13, pp. 511-517, 1978.

31. N. J. McEwan, et al., "OTS Propagation Measurements with Auxiliary Instrumentation," URSI Open Symposium on Effects of the Lower Atmosphere on Radio Propagation at Frequencies Above 1 GHz, Paper 6.2, Lennoxville, Canada, May 1980.

32. H. W. Arnold, D. C. Cox, H. H. Hoffman and R. P. Leck, "Characteristics of Rain and Ice Depolarization for a 19 and 28 GHz Propagation Path from a COMSTAR Satellite," IEEE Transactions on Antennas and Propagation, vol. AP-28, pp. 22-28, January 1980.

33. D. C. Cox, "Depolarization of Radio Wave by Atmospheric Hydrometeors in Earth-Space Paths," Radio Science, vol. 16, no. 5, pp. 781-812, September-October 1981.

34. H. W. Arnold and D. C. Cox, "Dependence of Depolarization on Incident Polarization for 19 GHz Satellite Signals," Bell System Technical Journal, vol. 57, pp. 3267-3276.

35. W. L. Stutzman, et al., "Final Report on Ice Depolarization on Satellite Radio Paths," Report prepared for International Telecommunications Satellite Organization, pp. 54-76, April 1981.

36. T. S. Chu, "Analysis and Prediction of Cross-Polarization on Earth Space Links," Ann. Telecommunic., vol. 36, no. 1-2, 1981.

37. C. W. Bostian and J. E. Allnutt, "Ice-crystal depolarization on satellite-earth microwave radio paths," Proceedings of the IEE, vol. 126, pp. 951-960, October 1979.

38. L. J. Battan, Radar Observations of the Atmosphere," revised edition, The University of Chicago Press, Chiago, 1973.

39. Alliss, D. N., et al., "An S-band Radar for Investigation of Rain and Ice Effects on Millimeter Wave Propagation," Interim Report 1981-1 prepared for NASA Headquarters under Contract NAS5-22577, Blacksburg, VA, November 1980.

Appendix A

BACKGROUND ON DEPOLARIZATION

Depolarization is the altering of an electromagnetic wave polarization. It is most often measured by either cross-polarization discrimination (XPD) or isolation. Isolation is defined as

$$\text{Isolation(dB)} = 20 \log \frac{|E_c|}{|E_x|} \tag{A.1}$$

where E_c is the electric field of the transmitted wave and E_x is the electric field of the wave with polarization orthogonal to that of E_c (called the cross polarized wave). This expression is general and holds for linear, circular or elliptical polarizations.

Depolarization is caused by two different sources. One is multipath propagation, which is limited to terrestrial links, and the other is hydrometeors along the propagation path. The latter cause is of primary interest here and will be discussed further. The two sources of hydrometeor propagation are rain and, ice crystals.

Rain induced depolarization was first studied using line-of-sight terrestrial microwave links. A good reference

of this early work does exist. [22] Measurements of rain-induced depolarization of a signal from Intelsat IV were reported in 1973. [23] Depolarization experiments were also conducted using the ATS-6 satellite (1975) and have continued up to the present with the COMSTAR, CTS and SIRIO satellites.

Nonspherical rain drops cause differential attenuation and phase shift which produces depolarization. The shape of these nonspherical raindrops tends to be that of an oblate spheroid. This is especially true as the size of the raindrop increases. For a volume of oblate spheroids of extent L (along the propagation direction) and canted at an angle of θ, the XPD's (or Isolations) are given as

$$XPD_V = 20 \log \frac{1 + \frac{T_2}{T_1} \tan^2 \theta}{\left(\frac{T_2}{T_1} - 1 \right) \tan \theta} \qquad (A.2)$$

for vertical polarization, and

$$XPD_H = 20 \log \frac{1 + \frac{T_2}{T_1} \tan \theta}{\left(\frac{T_2}{T_1} - 1 \right) \tan \theta} \tag{A.3}$$

for horizontal polarization. A similar expression exists for circular polarization. T_1 and T_2 are the transmission coefficients of the volume of oblate spheroids and are given as

$$T_1 = e^{-(A_1 - j\phi_1)L} \tag{A.4}$$

$$T_2 = e^{-(A_2 - j\phi_2)L} \tag{A.5}$$

A_1 and A_2 are the attenuation coefficients and ϕ_1 and ϕ_2 are the phase shift coefficients. [18] T_1 and T_2 have been determined, giving a complete solution to the XPD equation. [24] Thus, attenuation and phase measurements can be used to determine the XPD.

XPD can also be approximated using an empirical relationship. This is shown below.

$$XPD \simeq U - V \log(A) \tag{A.6}$$

A is the co-polarization attenuation. U and V are approximated by

$$U \simeq 20 \log \left[\frac{e^{-2\sigma_\phi{}^2 |\Delta K| \cos^2 \theta \sin(2|\phi - \delta|)}}{2} \right] \qquad (A.7)$$

$$V \simeq 20$$

where

$$\Delta K = \sqrt{(A_2 - A_1)^2 + (\phi_2 - \phi_1)^2} \qquad (A.8)$$

θ is the elevation angle, δ is the incident polarization tilt angle, and σ_ϕ is the standard deviation of the canting angle distribution. Again, attenuation measurements and phase shift measurements, along with the parameters specified above, are used to calculate the approximate value of XPD.

The CCIR has recommended the following approximations for V and U.

$$V \simeq 20 \qquad (A.9)$$

$$U \simeq 30 \log(f) - 40 \log(\cos \theta) - 20 \log(\sin|\phi - \delta|) \qquad (A.10)$$

where f, θ, ϕ and δ are the frequency in GHz, canting angle and polarization tilt angle, respectively.

Other empirical relationships between XPD and point rain rate have been proposed, but they have not yet been evaluated with measured data. [18]

Ice-crystal depolarization, also known as anomalous depolarization, takes place without the presence of significant co-polarized signal fading; only the cross-polarized signal changes significantly. It was first noticed in measurements made in 1974 using the ATS-6 satellite. Other experiments also conducted at frequencies above 10 GHz using the CTS, COMSTAR and SIRIO satellites have also produced further evidence of ice-crystal depolarization. Radar backscatter, when correlated with received satellite signals, has produced evidence of ice-crystal depolarization [25] In one instance, changes in radar backscatter were statistically correlated with fluctuations in XPD to produce evidence of ice-crystal depolarization. [23]

Measurement of depolarization, along an earth-space propagation path, begin in 1974 with the ATS-6 satellite. Ice-crystal depolarization was noticed in early experiments using ATS-6. [26] Other experiments using the ATS-6 satellite produced interesting characteristics of ice-crystal depolarization. One such characteristic is the relative phase

between the co-polarized and cross-plarized signals seems to stay constant, except for occcasional approximately 180 phase reversals. Another interesting observation was the strong correlation between lightning strokes and abrupt changes in XPD. [27] Ice-crystal depolarization was also observed in experiments using other satellites, such as COMSTAR and CTS. [28, 29]

More recent results have been reported. These involve experiments using COMSTAR, CTS and SIRIO satellites. Researchers have indicated that ice particle orientation is generally horizontal or vertical to the observation plane. [30] Experimenters using the COMSTAR satellite have confirmed that ice crystals are usually horizontally oriented. [31] Statistics on ice-crystal depolarization are needed for modeling. These include statistics on such parameters as frequency dependence, ice-crystal orientation and elevation angle. Reference [32] contains a good review of work done in these areas. Ice-crystal depolarization measurements have been improved by subtracting clear weather instrument residuals. Amplitude and phase of clear weather residuals signals can be measured. These residuals can be subtracted to correct measurements of hydrometeor induced depolarization. [33, 34]

Several models for ice-crystal depolarization do exist and work is continuing in the area. Some models are simple extension of the models for rain induced depolarization. For example, the XPD model proposed by Chu uses a 2 dB correction factor to compensate for ice-crystal depolarization. This gives a reliable prediction of XPD when compared to measured data. [35] Other models relate directly to the ice-crystal and receiving station parameters. For example, an XPD model exists that is a function of the volume of ice, the density of ice in the volume, the ice-crystal geometry, ice-crystal refractive index, frequency, the angle of incidence, Rayleigh scattering coefficients, polarization tilt angle and satellite elevation angle. This model gives good agreement with some measured results. [36] Work has continued in scattering theory applied to depolarization. A good review of work that has been done is available. [37]

Appendix B

RADAR METEOROLOGY

Radar was originally intended to be used for military purposes. Radars which were designed for detecting ships and planes were often impaired by clutter due to weather. This impairment was investigated in the 1940's and much of the theoretical and experimental groundwork in radar meteorology was performed. This early work has been developed further; radar backscatter can be used to determine the size, shape, orientation and motion of the backscattering hydrometeors, thus providing more information about meteorological events. For more information on radar meteorology and the development which follows, see reference [38].

The received power that is reflected from a target of cross section area A at a distance r is given by

$$P_r = \frac{P_t G A_t A_e}{(4\pi)^2 r^4} \tag{B.1}$$

where P_t is the transmitted power, A_e is the effective cross section of the antenna and G is the gain of the antenna. This assumed the target does not absorb any power and reradiates all incident power isotropically. The effective

aperture, A_e, of the antenna is given by

$$A_e = \frac{G \lambda^2}{4\pi} \tag{B.2}$$

and equation (B.1) can be written as

$$P_r = \frac{P_t G^2 A_t \lambda^2}{(4\pi)^3 r^4} \tag{B.3}$$

The target area, A_t, can be replaced by σ, which is the area, when multiplied by the incident power, gives the total power radiated by an isotropic source which radiates the same power in the reverse direction as the scatterer.

$$P_r = \frac{P_t G^2 \lambda^2 \sigma}{(4\pi)^3 r^4} \tag{B.4}$$

Equation (B.4) is general and can be applied to any target. For a large volume of scatterers, which is the usualy case, the backscattered power from the volume of randomly distributed scatterers is the sum of the power radiated by each scatterer, with phase taken into account. If the received backscattered power is averaged over a large sample of inde-

pendent volumes, the average power received is written as

$$\overline{P}_r = \frac{P_t G^2 \lambda^2}{(4\pi)^3 r^4} \sum_{i=1}^{N} \sigma_i \tag{B.5}$$

where the summation is for the volume of scatterers at any instant of time. The received backscattered power $\overline{P}_r$ can be rewritten as a backscattered power per unit volume, multiplied by a backscattering cross section volume, V_m. This assumes the scatterers are uniformly distributed in the volume. V_m is approximated as

$$V_m \simeq \pi r^2 \theta \phi \frac{h}{8} \tag{B.6}$$

where h is twice the volume depth, θ is the horizontal beamwidth, ϕ is the vertical beamwidth, and r is distance to the volume. Thus,

$$\overline{P}_r = \frac{P_t G^2 \lambda^2 \theta \phi h}{512 \pi^2 r^2} \sum_{Vol} \sigma_i \tag{B.7}$$

where the summation is now over a unit volume. This form of the radar equation contains assumptions about constant power across the beamwidth which lead to overestimates because the power decreases from the center of the beam and thus is not

constant. A more accurate expression for $\overline{P}_r$ can be written by assuming the power per unit area in the antenna main lobe can be approximated by a Gaussian form.

$$\overline{P}_r = \frac{P_t G^2 \lambda^2 \theta \phi h}{512 (2 \ln 2) \pi^2 r^2} \sum_{Vol} \sigma_i \qquad (B.8)$$

This is the basic form of the radar equation that is being used. All terms in Eq. (B.8), except the $\sum_{Vol} \sigma_i$ term, are known. Determining $\sum_{Vol} \sigma_i$ is a major concern in radar meteorology.

Mie scattering theory has been used to determine the backscattering cross section, σ, of a sphere. The expression for σ is given below.

$$\sigma = \frac{\pi a^2}{\alpha^2} \left| \sum_{n=1}^{\infty} (-1)^n (2n + 1)(a_n - b_n) \right|^2 \qquad (B.9)$$

where a is the sphere radius, α is equal to $2\pi a/\lambda$, a_n is related to scattering from an electric dipole, quadrupole etc. and b_n is related to scattering from a magnetic dipole, quadrupole, etc. The terms a_n and b_m can be expressed in terms of α, which is given above, and m, the complex index of refraction. For spheres with radii much smaller than the ra-

dar signal wavelength ($\alpha << 1$), σ_i can be expressed as

$$\sigma_i = \frac{\lambda^2}{\pi} \alpha^6 \left| \frac{m^2 - 1}{m^2 + 2} \right|^2 \tag{B.10}$$

Using $\alpha = 2\pi a/\lambda$ and letting $K = \frac{m^2 - 1}{m^2 + 2}$, σ_i can be rewritten as

$$\sigma_i = \frac{\pi^5}{\lambda^4} |K|^2 D_i^6 \tag{B.11}$$

where D_i is the diameter of the sphere. Now, $\overline{P}_r$ can be expressed as

$$\overline{P}_r = \frac{\pi^3}{1024 \ln 2} \frac{P_t G^2 \theta \phi h |K|^2}{\lambda^2 r^2} \sum_{Vol} D_i^6 \tag{B.12}$$

Equation (B.12) is the returned power from a region of spherical particles. This equation is for the case of Rayleigh scattering.

The term in equation (B.12) which represents the complex index of refraction is $|K|^2$ ($|K|^2 = \left|\frac{m^2 - 1}{m^2 + 2}\right|$). M is the complex index of refraction and is a function of both temperature and frequency. For centimeter wavelengths, $|K|^2$ for water and ice is essentially .93 and .20 respectively.

These values are for pure water and pure ice (no water). Combinations of ice and water give different results. Ice with a thin layer of water gives larger reflectivities than either ice or water.

The radar equation given in Equation (B.12) is derived assuming the backscattering particles are spherical. The problem of determining the actual backscattered power is much more complicated for non-spherical particles. The reflectivity is dependent on the shape and orientation of the scatterer. Also, for the non-spherical particles, the incident wave experiences depolarization. Early work in this area was performed in the 1950's. More recent developments in scattering theory have been reported. A good summary does exist. [37]

The radar equation in equation (B.12) is expressed in terms of D_i, the diameter of the $i^{\underline{th}}$ particle. The expression $\sum_{Vol} D_i$ is called the reflectivity factor. Z is the symbol that represents the reflectivity factor. The expression in equation (B.12)

$$\frac{\pi^3}{1024 \ln 2} \frac{P_t G^2 \theta \phi h}{\lambda^2} \qquad \text{(B.13)}$$

is a constant C for a radar system. Thus, equation (B.12)

can be expressed as

$$\overline{P}_r = C \frac{|K|^2}{r^2} Z \tag{B.14}$$

This equation assumes the beam is filled with scatterers.

The reflectivity factor Z is related to the drops in the contributing volume by

$$Z = \sum_{Vol} D_i^6 \tag{B.15}$$

This relatinship can be expressed in terms of the drop size distribution N(D). This is given in equation (B.16) as

$$Z = \sum_{Vol} D_i^6 = \int N(D)\ D^6\ dD \tag{B.16}$$

where N(D)dD is the number of scatterers per unit volume with diameters in the range from D to D+dD. The limits of integration in equation (B.16) are the minimum and maximum drop diameters. N(D) is called the drop-size distribution and for most rain and snow conditions it has an exponential form given as

$$N(D) = N_o\ e^{-\Lambda D} \tag{B.17}$$

where the quantities N_o and Λ are functions of the rain rate R in (mm/hr). For snow, the melted flakes are used in the distribution N(D).

Radar backscatter is related to the scatterers by Z and $|K|^2$. Since the reflectivity factor Z is a function of the distribution of the scatters, it can be used to make precipitation measurements. Z can be expressed in terms of the rain rate R given in (mm/hr). The relationship between Z and R is empirical and varies with storm type and geographic location. The general form is given in equation (B.18).

$$Z = A\, R^b \tag{B.18}$$

Many different values for A and b have been reported. Two sets of A and b values are given below. These are typical for the type of rain listed.

Stratiform rain	A = 200	b = 1.6
Thunderstorm rain	A = 486	b = 1.37

The A and b coefficients have also be empirically determined for snow. These correspond to equivalent rain rates that are calculated.

Thus, for a calibrated radar system, the received backscattered power $\overline{P}_r$ can be used to calculate Z. Z can be used to determine R, assuming a Z-R relationship exists for the radar system used. This technique is good for wavelengths greater than 10 cm. For wavelengths below 10 cm, attenuation causes a substantial reduction in backscattered power and must be taken into account.

Radar is also used to study other meteorological events. These include storm movement (thunderstorms, tornadoes, hurricanes and frontal precipitation, etc.), air turbulence, area rainfall measurement and ice detection. For a more in-depth discussion of these topics, see reference [38].

Appendix C

DEVELOPMENT OF THE DBZ EQUATION

The development of the radar equation was presented in Appendix B. This was done for the case of spherical scatterers. This spherical model will be used to analyze the radar data from each range gate. The form of the radar equation derived in Appendix B is not directly applicable; it must contain all system constants and be in a form that is easily put in computer code. The radar equation will now be put in the proper form. Only the major steps will be presented. A more thorough presentation is available. [39]

The basic radar equation for the Verlort S-band radar is given in Equation (C.1).

$$\bar{P}_r' = \frac{P_t G_1^2 G_2 G_3 G^2 \lambda^2 \sigma}{(4\pi)^3 r^4} \qquad (C.1)$$

The equation is for a single scatterer of backscattering cross-section σ. G_1, G_2, G_3 and G are gains in the radar system. The output of the log amp/integrator section is given in equation (C.2). This is for a coherent scatterer.

$$10 \log \bar{P}_r' = 10 \overline{\log P_r'} = A \cdot D - H + 2.5 \qquad (C.2)$$

A and H are constants obtained from a log amp calibration and D is a count (0 to 255) from the output of the log amp. Equation (C.1) can be used for calibration purposes. Substituting equation (C.2) in equation (C.1), the transmitter power P and the system gains can be obtained as a lumped parameter. This is shown in logarithmic form in equation (C.3)

$$10 \log[P_r G_1^2 G_2 G_3 G^2] = A_c D - H_c - 10 \log\left[\frac{\lambda^2 \sigma_c}{(4\pi)^3 r_c^4}\right] \quad \text{(C.3)}$$

The c subscript on A_c, D_c, H_c, σ_c and r_c correspond to calibration.

For a group of incoherent, random scatterers, the received power is given in equation (C-4).

$$\overline{P}_r = \frac{P_t G_1 G_2 G^2 \theta \phi h \pi^3 |K|^2}{1024 \ln(2) \lambda^2} \frac{Z}{r^2} \quad \text{(C.4)}$$

z is the radar reflectivity, θ and ϕ are antenna beamwidths

in radians, $|K|^2$ is a form of the complex index of refraction, λ is the wavelength in meters, and
pulse width in meters. Equation (C.4) can be solved for the reflectivity factor Z. This is shown in logarithmic form in equation (C.5).

$$10 \log Z = 10 \log \bar{P}_r - 10 \log[P_t G_1 G_2 G] - 10 \log \left[\frac{\theta \phi h \pi^3}{1024 \ln(2) \lambda^2} \frac{|K|^2}{r^2} \right] \quad (C.5)$$

Noting that

$$10 \log \bar{P}_r = 10 \log \bar{P}_r' - 10 \log G_1 G_2 \quad (C.6)$$

and that

$$10 \log \bar{P}_r' = A \cdot D - H + 2.5 - \frac{QI}{2} \quad (C.7)$$

equation (C.5) can be written as

$$10 \log Z = A \cdot D - H + 2.5 - \frac{QI}{2} - 10 \log[P_t G_1^2 G_2 G_3 G^2]$$

$$- 10 \log \left[\frac{\theta \phi h \pi^3}{1024 \ln(2) \lambda^2} \frac{|K|^2}{r^2} \right] \qquad (C.8)$$

Next, equation (C.3) can be substituted in (C.8) to give

$$10 \log Z = A \cdot D - H + 2.5 - \frac{QI}{2} - A_c \cdot D_c + H_c$$

$$+ 10 \log \left[\frac{\lambda^2 \sigma_c}{(4\pi)^3 r_c^4} \right] - 10 \log \left[\frac{\theta \phi h \pi^3}{1024 \ln(2) \lambda^2} \frac{|K|^2}{r^2} \right] \qquad (C.9)$$

Noting that $H = H_c$, $\theta = \phi = 2.5°$, $\lambda = 10.714$ cm and $h = 240$m, (C.9) can be put in a form that calculates dBZ for

each range gate j.

$$10 \log Z_j = A \cdot D_j - \frac{QI}{2} + 20 \log[1 + (j - 1)\ell]$$

$$- 10 \log|K|^2 - A_c \cdot D_c - 40 \log[1 + (j_c - 1)\ell_c] + 49.523 \qquad (C.10)$$

From a log amp calibration, $A = A_c = .251$. Also, $QI = .251$. A balloon-borne sphere was used to calibrate the radar system. This calibration employed a 6" (dia.) metal sphere. This was flown in range gate 8 ($\ell_c = .125$ km) and produced return counts D_c of 182. Using these calibration results,

$$10 \log Z_j = A \cdot D_j + 20 \log[1 + (j - 1)\ell] - 10 \log|K|^2 - 7.20 \qquad (C.11)$$

This form of the radar equation is suitable for computer coding and can be used to analyze the radar data.

Appendix D

COMPUTER PROGRAMS

```
//B0916R1L JOB 41036,RADAR,TIME=(20,00),TYPRUN=HOLD
/*LONGKEY CATHY
/*ROUTE PRINT MVS1.LOCAL
/*PRIORITY STANDARD
/*JOBPARM LINES=10
//STEP1 EXEC SAS,COND=EVEN
//INTAPE DD DISP=(OLD,KEEP),DSN=RADARDMP,
//   VOL=SER=2L07C,UNIT=TAPE16,LABEL=(1,SL),
//   DCB=(RECFM=FB,LRECL=1500,BLKSIZE=6000)
//DBZTAPE DD UNIT=TAPE62,DSN=RADAR.RLL.DATA01,
//   VOL=SER=EI98L,LABEL=(1,SL,,OUT),DISP=(NEW,KEEP)
//SYSIN DD *
*              RADAR1 SAS;
*THIS PROGRAM CONVERTS (0-255) TO DBZ VALUES,;
*CALCULATES SATELLITE  SIGNAL ISOLATION AND;
*ATTENUATION, AND STORES THEM ON TAPE EI98L.;
*(SEE JCL ABOVE.) THIS PARTICULAR PROGRAM HAS;
*THE CURRENT RADAR CALIBRATION CONSTANT(AS OF;
*1 APRIL 82) INCLUDED IN THE DBZ EQUATION.;
*THE VARIABLES IN THE PROGRAM ARE: L=RANGE;
*GATE LENGTH IN KM,KK=INDEX OF REFRACTION IN;
*DB,R=THE RADAR COUNT,J=THE RANGE GATE NO.;
*DBZ=THE RADAR REFLECTIVITY FACTOR IN DB,;
*CO AND CROSS ARE THE CO- AND CROSS-;
*POLARIZED SATELLITE SIGNALS;
TITLE RADAR DATA ANALYSIS;
DATA RADAN;
INFILE INTAPE;
L = 0.500 ;
KK = 0.315171 ;
AA=.2661556;
ARRAY R(J) R1-R128;
ARRAY DBZ(J) DBZ1-DBZ128;
INPUT DDAY  TIM TIME. R1-R128 CO CROSS W4 W58 W59 W9-W12 W61 W62;
IF DDAY=158;
IF 60. <= TIM <= 6300.;
ATTEN = 0;
DO OVER R;
IF J=1 THEN L=1.250;
ELSE L=0.500;
DBZ=R*AA + 20*LOG10(1+(J-1)*L) + KK + 5.81;
IF R <= 1 THEN DBZ=0.;
END;
IF CO< -130 THEN CO= . ;
IF CROSS< -150 THEN CROSS= . ;
ISOL = CO - CROSS+27.6;
DROP L KK AA ;
PROC MEANS DATA=RADAN MAX;
VAR CO;
OUTPUT OUT = XXXX
MAX = MX;
PROC PRINT ;
DATA DBZTAPE.RADAN2;
MERGE XXXX RADAN;
IF _N_ = 1 THEN MAXCO =MX;
RETAIN MAXCO;
ATTENM = MAXCO - CO;
N+1;
/*
//RELEASE EXEC RELEASE,JOBNAME=B0916R2L,COND=(0,NE)
//RELEASE EXEC RELEASE,JOBNAME=B0916R3L,COND=(0,NE)
//
```

```
//B0916RLL JOB 41036,RADAR,TIME=(01,00),TYPRUN=HOLD
/*LONGKEY CATHY
/*ROUTE PRINT MVS1.LOCAL
/*PRIORITY IDLE
/*JOBPARM LINES=5
//STEP1 EXEC SASV
//DBZTAPE DD DISP=(OLD,KEEP),DSN=RADAR.RLL.DATA01,
// VOL=SER=E198L,UNIT=TAPE62,LABEL=(1,SL)
//SYSIN DD *
GOPTIONS DEVICE=VPISASGV HSIZE=9 VSIZE=6.5;
********;
********;
*THIS PROGRAM COMPUTES THE PEARSON PRODUCT-;
*MOMENT CORRELATION COEFFICIENT FOR THE RANGE;
*GATES GIVEN (1 TO J). EACH GATE HAS 2 COEF;
*FICIENTS ASSOCIATED WITH IT, ONE FOR ATTEN-;
*UATION AND THE OTHER FOR ISOLATION. THESE;
*COEFFICIENTS ARE PLOTTED VS. RANGE GATE NO.;
*ATTENUATION AND ISOLATION ARE PLOTTED VS.;
*TIME ON A SEPERATE GRAPH. THE INPUT TO THIS;
*PROGRAM IS ON TAPE E198L (SEE DBZTAPE IN;
*JCL) AND COMES FROM THE PROGRAM RADAR1 SAS;
********;
********;
DATA XXXX;
ARRAY DBZ(J) DBZ1-DBZ128;
SET DBZTAPE.RADAN2;
IF DDAY=247;
IF 50283. <= TIM <= 50403.;
PROC CORR OUTP=KOR1 NOMISS;
VAR ATTENM ISOL CO CROSS;
WITH DBZ1-DBZ70;
DATA COR1;
SET KOR1;
KEEP ATTENM ISOL _NAME_;
IF _TYPE_ NE 'CORR' THEN DELETE;
DATA COREL;
SET COR1;
I+1;
KEEP ATTENM ISOL I;
* PLOT THE CORREATION COEFFICIENTS;
TITLE1 4 SEPTEMBER 1981;
TITLE2  CORRELATIONS FOR 13:58:03 TO 14:00:03;
PROC GPLOT GOUT=GRAPH6 DATA=COREL;
LABEL I=RANGE GATE;
LABEL ATTENM=CORRELATION COEFFICIENT;
SYMBOL1 C=BLACK V=A I=JOIN;
SYMBOL2 C=BLACK V=I I=JOIN;
PLOT ATTENM*I=1 ISOL*I=2/OVERLAY;
*PLOT ATTENUATION AND ISOLATION;
PROC GPLOT GOUT=GRAPH7 DATA=XXXX;
LABEL TIM=TIME IN GMT;
LABEL ATTENM=SIGNAL LEVEL IN DB;
FORMAT TIM TIME. ;
SYMBOL1 C=BLACK V=A I=JOIN;
SYMBOL2 C=BLACK V=I I=JOIN;
PLOT ATTENM*TIM=1 ISOL*TIM=2/OVERLAY;
TITLE1 4 SEPTEMBER 1981;
TITLE2 ATTENUATION AND ISOLATION VS. TIME;
DATA ALL;
SET GRAPH6 GRAPH7;
PROC GREPLAY DATA=ALL;
```

```
//B0916RLL JOB 41036,RADAR,TIME=(01,00),REGION=750K
/*LONGKEY CATHY
/*PRIORITY IDLE
/*ROUTE PRINT MVS1.LOCAL
/*JOBPARM LINES=20
//STEP1 EXEC SASV,REGION=750K
//DBZTAPE DD DISP=(OLD,KEEP),DSN=RADAR.RLL.DATA01,
//   VOL=SER=E198L,UNIT=TAPE62,LABEL=(1,SL)
//SYSIN DD *
GOPTIONS DEVICE=VPISASGV HSIZE=9 VSIZE=6.5;
********;
********;
*                GATEPLT SAS                *;
*THIS PROGRAM PLOTS MEASURED ATTENUATION,ISOLATION,;
*AND BACKSCATTER (DBZ) VS. TIME. THIS CAN BE DONE;
*FOR TWO SPECIFIED RANGE GATES. THE INPUT TO THIS;
*PROGRAM IS ON TAPE E198L (SEE DBZTAPE IN JCL) AND ;
*COMES FROM THE PROGRAM RADAR1 SAS.;
********;
********;
DATA THRDIM;
ARRAY DBZ(J) DBZ1-DBZ20;
SET DBZTAPE.RADAN2;
I=0;
IF DDAY=266;
IF 65820. <= TIM <= 66120.;
DO OVER DBZ;
I+1;
Z=DBZ;
IF Z < 0. THEN Z=0.;
KEEP TIM I Z ISOL ATTENM;
OUTPUT;
END;
DATA PLOT1;
SET THRDIM;
************ SPECIFY THE GATE NO. ************;
IF I=11;
TITLE1 22 SEPTEMBER 1980;
TITLE2 GATE 11, Z,ATTEN AND ISOL VS. TIME;
PROC GPLOT GOUT=GRAPH1;
LABEL TIM=TIME IN GMT;
LABEL Z=SIGNAL LEVEL IN DB;
FORMAT TIM TIME. ;
SYMBOL1 C=BLACK V=Z I=JOIN;
SYMBOL2 C=BLACK V=I I=JOIN;
SYMBOL3 C=BLACK V=A I=JOIN;
PLOT Z*TIM=1 ISOL*TIM=2 ATTENM*TIM=3/OVERLAY;
DATA PLOT2;
SET THRDIM;
************ SPECIFY THE GATE NO. ************;
IF I=17;
TITLE1 22 SEPTEMBER 1980;
TITLE2 GATE 17, Z,ATTEN AND ISOL VS. TIME;
PROC GPLOT GOUT=GRAPH2;
LABEL TIM=TIME IN GMT;
LABEL Z=SIGNAL LEVEL IN DB;
FORMAT TIM TIME. ;
SYMBOL1 C=BLACK V=Z I=JOIN;
SYMBOL2 C=BLACK V=I I=JOIN;
SYMBOL3 C=BLACK V=A I=JOIN;
PLOT Z*TIM=1 ISOL*TIM=2 ATTENM*TIM=3/OVERLAY;
DATA ALL;
SET GRAPH1 GRAPH2;
PROC GREPLAY DATA=ALL;
/*
//
```

The vita has been removed from the scanned document

STATISTICAL CORRELATION AS A TOOL IN PROPAGATION STUDIES

by

Robert L. Lyall, Jr.

(ABSTRACT)

This thesis investigates statistical correlation as a means to enhance the use of ground-based radar in analyzing satellite-path millimeter wave propagation through rain and ice crystals. The technique presented involves correlating dB values of the satellite signal attenuation and polarization isolation with dBZ values of radar backscatter from each of 128 range gates. In it, Pearson product moment correlation coefficients are calculated for attenuation and backscatter and for isolation and backscatter. When these coefficients are plotted versus radar range, one of four certain characteristic patterns usually appears.

Ice-crystal depolarization produces a pattern of near zero attenuation coefficients and varying isolation coefficients. Rain produces a correlation pattern in which the attenuation coefficient pattern is nearly mirror image of the isolation coefficient pattern. A special case of the rain event occurs when the cross-polarized satellite signal is essentially constant. The correlation patterns for this case are exact mirror images. Rain attenuation and depolarization accompanied by additional depolarization from anoth-

er source, produce a correlation pattern that is not symmetrical. This is due to the additional depolarization. Discussion of these expected patterns and examples of each are presented.